Simulation-based high resolution fire danger mapping using deep learning

Frédéric Allaire, Jean-Baptiste Filippi, Vivien Mallet, Florence Vaysse

▶ **To cite this version:**

Frédéric Allaire, Jean-Baptiste Filippi, Vivien Mallet, Florence Vaysse. Simulation-based high resolution fire danger mapping using deep learning. International Journal of Wildland Fire, 2022, 31 (4), pp.379-394. 10.1071/WF21143 . hal-03189847

HAL Id: hal-03189847

https://inria.hal.science/hal-03189847

Submitted on 5 Apr 2021

HAL is a multi-disciplinary open access archive for the deposit and dissemination of scientific research documents, whether they are published or not. The documents may come from teaching and research institutions in France or abroad, or from public or private research centers.

L'archive ouverte pluridisciplinaire **HAL**, est destinée au dépôt et à la diffusion de documents scientifiques de niveau recherche, publiés ou non, émanant des établissements d'enseignement et de recherche français ou étrangers, des laboratoires publics ou privés.

Simulation-based high resolution fire danger mapping using deep learning

Frédéric Allaire[A], Jean-Baptiste Filippi[B,*], Vivien Mallet[A], and Florence Vaysse[C]

[A] Institut national de recherche en informatique et en automatique (INRIA), 2 rue Simone Iff, Paris, France; Sorbonne Université, Laboratoire Jacques-Louis Lions, France.

[B] Centre national de la recherche scientifique (CNRS), Sciences pour l'Environnement – Unité Mixte de Recherche 6134, Università di Corsica, Campus Grossetti, Corte, France.

[C] Météo-France, Centre régional Sud-Est, 2 bd Château Double, Aix-en-Provence, France.

[*] Email: frederic.allaire@inria.fr; corresponding author.

Abstract: Wildfire occurrence and behavior are difficult to predict very locally for the next day. In the present work, we use an artificial neural network emulator called DeepFire, trained on the basis of simulated fire sizes, and study its application to fire danger mapping using actual weather fore-

casts. Experimental analysis is based on DeepFire forecasts for 13 relatively big fires that occurred in Corsica and corresponding forecasts based on a fire danger index used in operational conditions. A comparative analysis of both indices is presented, highlighting the differences in terms of precision and expected results of such predictions. Forcing weather forecasts used as input have high spatial resolution and high frequency, which also applies to the fire danger predictions. Additionally, input uncertainty is propagated through DeepFire, resulting in ensembles of emulated fire size. Eventually, several approaches are proposed to analyze the results and help in investing assessment of next-day fire danger using this new simulation-based prediction system.

Keywords: wildfire simulation, deep learning, fire danger, potential fire size, fire weather, probability distributions

1 Introduction

Wildfire occurrence and behavior is difficult to predict accurately. The environmental conditions such as weather and the type(s) of vegetation involved may be known to some extent, but the time, location, and cause of fire occurrence are rarely known ahead of time. A common approach in wildfire prediction consists in assessing fire danger, a general term that expresses both fixed and variable factors of the fire environment that influence the ease of ignition, rate of spread and difficulty of control.

Fire danger rating systems include assessment of one or several fire danger indices, which are used among other information to provide a rating, i.e. a class whose possible values may include “low”, “moderate”, “severe”, “extreme”, etc., but the notion of “rating” may also refer to the scalar indices composing the system. Regardless of the type of quantity used to assess it, fire danger relates to the proneness for ignition, spread and/or intensity of a wildfire according to the state of the vegetation and its environment at a given time, therefore reflecting how difficult it may be to control fire. Development of fire danger rating methods has led to the implementation of systems at the national scale about 50 years ago in Canada and in the US, with the Canadian Forest Fire Danger Rating System (CFFDRS Lawson and Armitage (2008), whose development started in 1968) and the National Fire Danger Rating System (NFDRS Bradshaw et al. (1984), first published in 1972, but whose development as well as fire danger rating methods dates

further back, see for instance Hardy and Hardy (2007)).

Maps of fire danger ratings are usually generated every day to assess the situation of the current day and forecast the situation for the day(s) to come. Such maps may be available among other data via internet-based information systems; for instance, covering the US as part of the Wildland Fire Assessment System (WFAS Burgan et al. (1997))[1], covering Canada as part of the Canadian Wildland Fire Information System (CFWIS)[2], covering Europe and the Mediterranean area as part of the European Forest Fire Information System (EFFIS)[3], or even covering the globe as part of the Global Wildfire Information System (GWIS)[4], which builds on activities of EFFIS.

Calculation of the aforementioned fire danger indices mostly depends on weather inputs and, to some extent, fuel moisture, which is generally derived from weather information. In the CFFDRS, the final output is a composite Fire Weather Index (FWI), that depends on such inputs, more precisely wind speed, air temperature, relative humidity and rainfall over the previous 24 hours, as well as the values of the indices from the day before. Although one could consider computing the indices at high temporal resolution, they are generally computed to represent peak, or at least high, fire weather conditions in a given day. Also, although the FWI was calibrated to describe fire behav-

[1] https://www.wfas.net/, last checked 2021.02.01
[2] https://cwfis.cfs.nrcan.gc.ca/maps/fw, last checked 2021.02.01
[3] https://effis.jrc.ec.europa.eu/, last checked 2021.02.01
[4] https://gwis.jrc.ec.europa.eu/, last checked 2021.02.01

ior in a jack pine stands, it has been implemented in many other countries despite the differences in vegetation and climate where it showed reasonable performance (see for instance Giuseppe et al. (2020) and references therein). Forecasted maps of such indices generally have a temporal resolution of one day even if the underlying weather forecasts have higher temporal resolution, but the temporal extent and spatial resolution are generally the same.

Weather forecasts covering a smaller area may have higher spatial resolution: for instance the regional AROME limited area model in use at Météo-France has a spatial resolution of 1.3 km, covers France and part of neighboring countries, and allows for the computation of fire danger index at much higher resolution. AROME is also an operational system used as a reference in this study. Meteorological assistance for forest fires started in the 60s and the Météo-France methodology has been gradually evolving over the years, depending on the research but also on the feedback of the various departments of Civil Protection and the ONF who fight against forest fires.

In summer, the Mediterranean vegetation is evolving between a growth phase in spring to a dormancy phase between mid-summer and early fall. When the scrubland's shrubs are falling over to this vegetative state, there is a very small quantity of water in leaves and thus the Mediterranean vegetation is becoming extremely flammable by dry weather. The expertise of weather fire danger requires, firstly, the monitoring of drought to evaluate whether or not the vegetation is prone to big summer fires.

In this configuration, at Météo-France, the forecaster assesses weather fire

danger with 3 main indices; FWI: for vegetation in low or moderate drought, IPse: a local rate of spread index for very dry vegetation and IEP (Indicateur d'éclosion et Propagation, French for "Ignition and spread indicator"): for dead or dormancy vegetation for which the water content is directly linked with air moisture and therefore Fine Fuel Moisture Content (FFMC). All those indices are calculated at the maximum of the day based on hourly values (in which case, they are post-fixed with an x, leading to FWIx, IPsex, and IEPx). Weather fire danger depends on wind speed and highest temperatures/lowest air moisture, which can happen at different moments during the day depending on the local meteorological context; for instance, strong and dry winds can happen at any moment in the day and even in the night in Mediterranean areas.

Instead of relying on empirically calibrated formulas to compute indices that are, for the most part, unitless, a promising strategy is to rely on a large number of simulations of fire spread using weather forecasts as input, therefore providing a more "concrete" representation of fire spread via simulated burned surfaces. Two interesting methods following such a strategy, although applied at different time scales than day to day predictions, are burn probability (BP) modeling and ensembles of simulations for specific fire cases.

BP modeling consists in propagating input distributions of environmental characteristics (weather and fuels) and fire characteristics (ignition, fire duration, number of fires in a year) via several simulations of wildland fire

ignition and spread, this process being repeated independently several times via a MC method to represent potential scenarios of wildland fire activity in a region and/or a country. In this context, the output BP maps represent the probability of local areas to be burned by a fire (typically over the course of a year). Notable implementations include Burn-P3 Parisien et al. (2005) which relies on the Prometheus solver Tymstra et al. (2010) and FSim Finney et al. (2011b) which relies on FARSITE Finney (1998). A large number of studies have proposed and/or applied BP modeling (see for instance Parisien et al. (2019) and references therein).

Similarly, ensembles of simulations for specific fire cases allow to assess "burn probabilities", following a Monte Carlo approach that accounts for input uncertainty in fire spread simulations, notably regarding weather variables. A notable implementation of this method is the FSPro system Finney et al. (2011a), which relies on an ensemble of FARSITE simulations. Due to knowledge of the ignition location, the burn probability maps resulting from such ensembles cover a much smaller area than maps of BP modeling.

From an operational perspective, BP modeling can be seen as a decision support tool for "long-term" planning, whereas ensembles of simulations for specific fire cases apply to "crisis" situations. In "short-term" predictions, however, the input distributions should be more representative of the expected weather conditions as in ensembles of simulations for specific fire cases, but should also account for the lack of knowledge regarding future ignitions over a vast territory, as in BP modeling. Although BP modeling

methods could be adapted to account for daily weather forecasts, their computational requirement due to the large number of simulations involved is too high for use in an operational context.

The approach developed in this work proposes to use wildland fire simulations as basis for short-term assessment of fire danger, while relying on deep learning to reduce the computational cost of running a high number of simulations. A deep neural network (DNN) referred to as *DeepFire* in the following is used to approximate the potential fire size returned by a fire spread simulator.

DeepFire is able to compute a high number of fire size estimations in a short amount of time, and could generate fire danger maps at both high spatial resolution (approximately 80 m) and high frequency (10-minute time step) in a operational context. The fire size computations could be obtained using a fire spread simulator, but would require several days in this context. Compared to traditional fire danger indices, two major differences of DeepFire are that it accounts not only for weather but also for the influence of terrain on fire spread, and that fire danger is expressed as a physical quantity, namely a surface area (in hectares). Its output and overall design are therefore quite different from the CFFDRS, for instance. It is also possible to run an ensemble of DeepFire predictions to quantify uncertainty, although at lower spatial resolution (640 m). Compared to BP modeling, a noteworthy difference is that DeepFire focuses on "sources" of fire spread (i.e. how large will be the burned surface, assuming that an ignition will occur at a specific

location), while burn probabilities represent "sinks" of fire spread (i.e. how often a specific location is likely to be burned, as a result of several scenarios of fire spread each with variable ignition location).

A key aspect of this work is the the availability of high-resolution weather forecasts, which is arguably a major limitation for application of a BP approach to short-term predictions. In the frame of this study, a limited-area model running at 600-m resolution is used to generate a forecast of surface wind, fuel moisture, and air temperature with a time extent of 42 hours. In order to be representative of operational applications, this high-resolution weather forecast was run daily (at midnight) from 10/05/2017 and was available around 11:00. To account for rapidly changing conditions, a high-frequency simulation output with a time step of 10 minutes is provided, resulting in time-series of 253 spatial fields of weather variables, which are forecasted every day.

Section 2 details the method that is used to obtain predictions of fire danger with DeepFire and with IEP. Analysis of forecasts for days were relatively large fires occurred is presented in Section 3. A detailed analysis is first provided for one fire, then more synthetically for 12 other fires. Section 4 addresses the question of generating daily maps that indicate the danger for the coming day in order to summarize the high number of maps resulting from the high forecast frequency. Finally, the main conclusions of this study and some perspectives are given in Section 5.

2 Method

2.1 DeepFire: fire size emulation using a deep neural network

The new approach proposed to quantify fire danger consists in predicting, for a given time and location, the size of the burned surface that would result from one hour of free wildfire spread after an early stage where the fire has already ignited and spread over about one acre. Ignition probability is assumed homogeneous, except for locations without vegetation where it is considered null. A duration of one hour is generally more than the time necessary for the first attack on the fire to be carried out, even more so if one assumes that the fire has been detected in the early stage. These simplifying assumptions imply that fire danger mostly expresses potential for fire spread if it is not attacked rather than potential for ignition.

In the present study, the one-hour fire size is estimated using the DNN *DeepFire*. Its architecture is "hybrid" in the sense that it has two types of input data. The first type is similar to an image: it is composed of four rasters describing the landscape with a spatial resolution of about 80 m in a square of 20 km × 20 km centered around the ignition location. One raster represents elevation and the other three are derived from the same land cover data. Aside from non-burnable areas, each type of land use is matched with a fuel behavior model, for a total of 13 different fuel models. The three fields other than elevation therefore represent the variable parameters of the fuel

Input	Symbol	Unit	Type	Range	Constraint
Wind speed	(W_x, W_y)	$\mathrm{m\,s^{-1}}$	Raw	$[-35, 35]^2$	Euclidean norm ≤ 35
Fuel moisture content (dead fuel)	m_c		Raw	$[0.04, 0.3]$	
Heat of combustion perturbation	ΔH	$\mathrm{MJ\,kg^{-1}}$	Additive	$[-5, 5]$	
Particle density perturbation	ρ_p	$\mathrm{kg\,m^{-3}}$	Additive	$[-300, 300]$	
Fuel height perturbations	h	m	Multiplicative	$[0.4, 1.6]^{13}$	
Fuel load perturbations	σ_f	$\mathrm{kg\,m^{-2}}$	Multiplicative	$[0.4, 1.6]^{13}$	
Surface-volume ratio perturbations	S_v	$\mathrm{m^{-1}}$	Multiplicative	$[0.4, 1.6]^{13}$	
Relative ignition point coordinates	$(\delta x, \delta y)$	m	Raw	In a fuel cell	

Table 1: Scalar inputs of DeepFire. In the case of perturbations, the symbol corresponds to the perturbed quantity, and the perturbation of this quantity can be either additive or multiplicative. The range indicates the boundaries of the domain of definition with two components for the wind and 13 components in the last three rows (one row per fuel type).

models, namely, the height h, the load σ_f, and the surface-volume ratio S_v. The second type or inputs are scalars, listed in Table 1, that describe physical quantities influencing fire behavior: the wind speed vector (W_x, W_y), the FMC m_c, and coefficients used to perturb the default values of fuel model parameters. Two fuel parameters, namely the heat of combustion ΔH and the particle density ρ_p, have the same default value for all fuel models and only have one additive perturbation coefficient each. The other parameters (h, σ_f, and S_v) depend on the fuel model and each have one multiplicative perturbation coefficient per fuel type, which, including the previous two coefficients, amounts to 41 perturbation coefficients. The remaining scalar inputs are two coordinates that locate the ignition point inside the fuel cell of the land cover raster where fire starts, but given the small size of the fuel cells, these two inputs barely have any influence on fire size estimation.

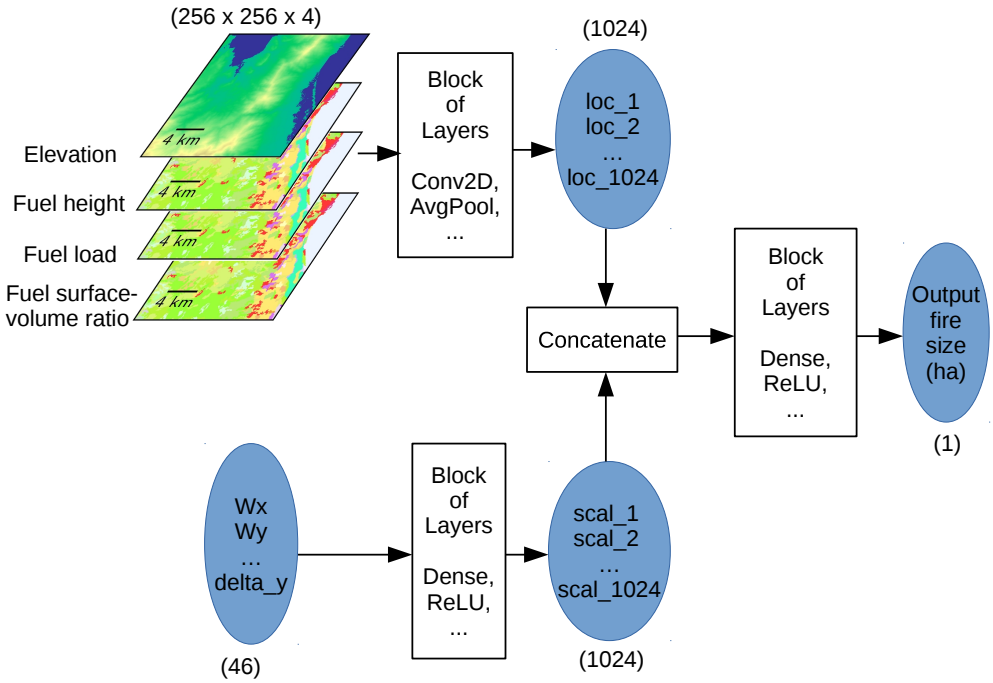

Figure 1: Architecture of the DeepFire neural network.

Each type of input is first processed differently by DeepFire, a summarized representation of the neural network architecture being shown in Figure 1. Several convolutional layers and average pooling layers (among others) are applied to the rasters while the scalars mostly go through a dense layer and a rectified linear unit (ReLU) layer. This results in two intermediate vectors of size 1024: the first vector only depends on the terrain around ignition point, whereas the second vector depends on the scalar inputs. The rest of the network consists in concatenating both vectors, and applying several dense and ReLU layers, for finally providing an estimate of the fire size. The parameters of the network were fitted so that DeepFire returns a good approximation of the one-hour fire size that would be simulated by the fire spread solver ForeFire Filippi et al. (2010) using the rate of spread model of Rothermel Rothermel (1972) with the same inputs. In the simulations, the initial burned surface is a 0.45-ha octagon, which is also the minimum returned by both ForeFire and DeepFire (this generally happens when the FMC is close to the moisture of extinction). DeepFire is an emulator (aka, metamodel or surrogate model) of the one-hour fire size returned by ForeFire, that is to say a model that computes this output considerably faster. The first intermediate vector of "location" is pre-computed for each fuel cell in the region studied (about 1.2 million fuel cells for Corsica island). Based on these pre-computed vectors, the one-hour fire size can be computed for all cells in about one minute for any ignition location, which is thousands of times faster than with ForeFire and makes daily fire danger mapping

in operational conditions technically possible. More details on the neural network and its use for emulation of fire spread simulation can be found in Allaire et al. (2021a).

2.2 Deterministic predictions of fire danger maps

The design of DeepFire allows for fire danger mapping of Corsica island at high spatial resolution. First, for a given fuel cell, the intermediate location vector (that was pre-computed) is used as input of the concatenate block. The ignition point is assumed to be located at the center of the fuel cell, which defines δ_x and δ_y. Then, scalar fuel parameters perturbations are set to 0 and 1 for additive and multiplicative coefficients, respectively, which corresponds to no alteration of the default values of the fuel model parameters. Finally, wind speed and FMC are quantities that vary during the day, so they are estimated based on a weather forecast. A spatial interpolation can be carried out to determine the value of these three inputs at the center of a given fuel cell to address differences in spatial resolution and/or coordinate system (in the present study, a barycentric interpolation is used). In extreme cases where the wind speed norm is higher than $35\,\mathrm{m\,s^{-1}}$, wind speed is reduced to this threshold because DeepFire was not trained based on simulations outside this scope. Similarly, when the FMC is lower than 0.04, this lower bound is used as input of DeepFire. Also, the minimum output value (0.45 ha) is automatically returned when the FMC is higher than 0.3, which is the moisture of extinction used in ForeFire simulations. The computation of the

DeepFire output with the aforementioned inputs corresponding to each fuel cell of the map and each forecast time of the weather forecast results in a time sequence of fire danger maps at high spatial resolution. Given that no perturbations are applied to the scalar inputs, this is referred to as a *deterministic prediction* of fire danger in the following.

Wind speed \ FFMC	≤ 80	]80, 85]	]85, 89]	]89, 93]	]93, 96]	> 96
$\leq 10\,\mathrm{kt}$	low (1)	low (1)	minor (2)	moderate (3)	severe (4)	severe (4)
]10 kt, 20 kt]	low (1)	minor (2)	moderate (3)	severe (4)	severe (4)	very severe (5)
]20 kt, 30 kt]	low (1)	minor (2)	moderate (3)	severe (4)	very severe (5)	very severe (5)
$> 30\,\mathrm{kt}$	minor (2)	moderate (3)	severe (4)	very severe (5)	very severe (5)	very severe (5)

Table 2: Computation of the IEP based on the norm of wind speed (in knots) and the FFMC.

Using the same weather forecast as for DeepFire, a time sequence of fire danger maps at high spatial resolution based on the IEP can be obtained similarly. IEP is one of the operational danger rating indicator in France that serves for both summer and winter. The design of IEP is mostly empirical and based on phenological assumptions. In the autumn, as soon as days become shorter and temperatures lower, the vegetation transforms itself again. Deciduous trees lose their leaves which accumulate on soil and the forest litter thicken. Other trees, shrubs and bushes 'hibernate' and become in dormancy with a very low quantity of sap/water in their leaves. At the same time, herbaceous are at the end of their cycle and die. In addition to this traditional and seasonal dormancy, with climate warming, more and more vegetation dies with huge and record summer drought. The dead or

dormancy vegetation water content is directly linked with air humidity (as a sponge effect). In this case, the IEPx (daily maximum) is the most relevant indicator. In the 2010s, some huge fires occurred with moderate or just severe weather fire conditions in places where dead vegetation were numerous. By studying indices and conditions in a file constituted by more than 5000 summer alerts from 2001, Météo-France set up an indicator by crossing FFMC, correlated with outbreak potential, and wind. Since then, by empiricism and following winter and summer situations, with Fire Brigades and National Forest officers, it was concluded that this indicator was the most relevant indicator for winter fires and a good complement in summer for dead or dormancy vegetation in very dry conditions (as it was the case in summer 2017 in Corsica).

The IEP has five possible categories ranging from "low" to "very severe" that only depend on the norm of wind speed and the FFMC as determined from Table 2. Let us underline that both FMC and FFMC are diagnostic variables of the weather forecast, i.e. they are deduced from the other variables. The FFMC is generally based on the forecast for 12:00 in local time, but this method does not account for variations of fuel moisture during the day, whereas the forecasted FMC used as input of DeepFire may vary over time. For consistency, we decided not to compute the input FFMC of the IEP in the "standard" way but based on the value of FMC m_c, according to

Equation (2.1):

$$\mathrm{FFMC} = 59.5 \times \frac{250 - m_c}{147.2 + m_c}, \tag{2.1}$$

which is the final equation intervening in calculation of the FFMC in the Canadian system (cf. Equation (10) in Van Wagner and Pickett (1985), where the other equations are used to provide an estimate of m_c).

Fire size (ha)	< 0.1	[0.1, 4.0[	[4.0, 40.5[	[40.5, 121.4[	[121.4, 404.7[	[404.7, 2023.4[	≥ 2023.4
Category	A	B	C	D	E	F	G
Corresponding IEP	None	low (1)	minor (2)	moderate (3)	severe (4)	very severe (5)	very severe (5)

Table 3: Values of fire sizes used to determine a class of fire danger. The fire size classes follow the US classification and a correspondence of fire danger classes was made between DeepFire and IEP in the present study.

Categories of DeepFire values were determined based on thresholds of burned surface area to provide maps with a categorical color scale for easier interpretation. For simplicity, the thresholds of the US classification of fire size[5] were chosen, providing seven categories ranging from A to G, as reported in Table 3. This choice is not perfectly suited to DeepFire which estimates the one-hour fire size of a freely spreading wildfire, whereas the US classification accounts for all observed fires, even if there were firefighting actions or the fire did not last one hour. The minimum value returned by ForeFire is 0.45 ha, which implies that class A will not be obtained in the present study at all. Similarly, class G should be quite rare as it is only returned by

[5] https://www.nwcg.gov/term/glossary/size-class-of-fire, last accessed on 2020.12.11

DeepFire given extreme input conditions (very high wind speed and very low FMC). Still, classes B to F should all contain at least a fair proportion of DeepFire predictions so this choice, although arbitrary, makes sense as a first approach. In practice, the thresholds should be calibrated in order to provide a fire danger indicator that is as relevant as possible. Finally, for qualitative comparison of danger class predicted by DeepFire and IEP, a correspondence reported in Table 3 was made.

2.3 Probabilistic predictions representing input uncertainty

A major aspect that is not accounted for by the deterministic predictions is the uncertainty associated to the modelling process, that could lead to a difference between the "actual" one-hour fire size that would be observed and its estimate. Although it may not be possible to determine the actual value (firefighting actions usually occur, it can be difficult to measure, etc.), several sources of uncertainty can be identified such as the error of approximation between DeepFire and ForeFire and simplifying model assumptions. Arguably, the main source of uncertainty regarding DeepFire predictions stems from the weather predictions and values of fuel model parameters, that is to say input uncertainty.

Previous studies Allaire et al. (2020,2) focused on the quantification of input uncertainty in simulations of wildland fire spread. To quantify the

uncertainty in the inputs of DeepFire, we use a *calibrated* probability distribution associated to the inputs of ForeFire simulations. The calibration method is detailed in Allaire et al. (2021b); its key aspect consists in using an *a priori* distribution where the marginals of each individual input have higher variance than in Allaire et al. (2020) and including the information of observed burned surfaces of seven Corsican fires. The *probability density function* (PDF) g of the calibrated distribution is intended to be higher than the prior PDF f for a given input vector $\boldsymbol{u}$ when there is good overall agreement between observed burned surface $\mathcal{S}_{\text{obs}}$ and corresponding simulated burned surface $\mathcal{S}_{\boldsymbol{u}}$. More precisely, the PDF g can be expressed as follows:

$$g(\boldsymbol{u}) = \frac{e^{-\beta E(\boldsymbol{u})} f(\boldsymbol{u})}{\int e^{-\beta E(\boldsymbol{u})} f(\boldsymbol{u}) d\boldsymbol{u}}, \tag{2.2}$$

where $\beta > 0$ and E is a positive "energy" function that is equal to 0 when $\mathcal{S}_{\boldsymbol{u}} = \mathcal{S}_{\text{obs}}$ for each fire and increases with the dissimilarity between simulated and observed burned surfaces. Measurement of shape dissimilarity relies on the Wasserstein distance, which is a metric that appears in the field of optimal transport (see, for instance, Santambrogio (2015) for an extensive review), and $E(\boldsymbol{u})$ can be understood as an energy that is required to transform $\mathcal{S}_{\boldsymbol{u}}$ into $\mathcal{S}_{\text{obs}}$. The definition of g is inspired from Bayes' rule:

$$p(\boldsymbol{u}|\mathcal{S}_{\text{obs}}) = \frac{\mathcal{L}(\mathcal{S}_{\text{obs}}|\boldsymbol{u}) f(\boldsymbol{u})}{\int \mathcal{L}(\mathcal{S}_{\text{obs}}|\boldsymbol{u}) f(\boldsymbol{u}) d\boldsymbol{u}}, \tag{2.3}$$

where $p(.|\mathcal{S}_{\text{obs}})$ is the posterior PDF that would be obtained from $\mathcal{L}(\mathcal{S}_{\text{obs}}|.)$,

the likelihood of the observation, and f, the prior PDF. The exponential in Equation (2.2) can therefore be seen as a pseudo-likelihood function, whose weight increases with the parameter β. When $\beta = 0$, the calibrated PDF g is equal to the prior PDF f.

In the present study, the calibrated input distribution obtained with $\beta = 1/2$ is used. The components of the input vector $\boldsymbol{u}$ are similar to the scalar inputs of DeepFire listed in Table 1. The perturbations in fuel parameters are exactly the same and can be used directly as input of DeepFire instead of the values 0 and 1 used for the deterministic prediction. Regarding wind speed and FMC, however, the corresponding components of $\boldsymbol{u}$ are perturbation coefficients so that each value of W_x, W_y, and m_c in the weather forecast is perturbed using the corresponding components of $\boldsymbol{u}$. As for the deterministic prediction, a threshold is applied so that the perturbed value of wind speed norm and FMC fall in the range used to train DeepFire. By sampling n independent sets of perturbation coefficients $(\boldsymbol{u}_1, ..., \boldsymbol{u}_n)$ following the calibrated distribution, one may obtain n replicas of the deterministic DeepFire predictions but using perturbed inputs so that each of these n predictions is different. The resulting ensemble of n DeepFire predictions is referred to as a *probabilistic prediction* in the following.

A probabilistic prediction based on a large ensemble can be fairly easily obtained when one considers a single ignition location. However, computing an ensemble of M high-resolution maps requires M times more computational time, making the generation of a representative ensemble too long for

operational context conditions. To circumvent this issue, the spatial resolution of the fire danger maps can be reduced. For each large cell and each forecast time, we define a "representative cell": the small cell which has the highest DeepFire value according to the deterministic prediction. For each large cell, the computations of the probabilistic prediction is only carried out for the small representative cell. In case the large cell contains a high number of non-burnable cells, it may be considered as non-burnable as well (here, it is considered to be the case when at least 90% of the cells are non-burnable). It must also be noted that these ensembles are distinct from atmospheric forecast ensembles, while the later may also be used as inputs for these simulations to account for weather uncertainties, all fire danger predictions for a given day in the present study, whether deterministic or probabilistic, were based on a single deterministic weather forecast.

2.4 Application to weather forecasts corresponding to 13 Corsican fires

Daily forecasts are generated with a high-resolution run of the limited area model Meso-NH version 5.4 Lac et al. (2018). While being the support of coupled fire/weather simulations, Meso-NH is also the atmospheric research model of the French community, maintained and developed by two laboratories associated on the research program (Centre National de la Recherche Scientifique and Laboratoire d'Aérologie) that provided access to opera-

tional runs providing the boundary and initial conditions. Boundary and initial conditions are gathered from the Météo-France archive of the AROME model Amodei et al. (2015). The 00Z run is downloaded daily from the system and is available at around 3AM. The daily computation is performed by Meso-NH on a Cartesian regular grid at 600 meter resolution and 46 atmospheric levels (up to an altitude of 7000 meters). In the application over Corsica this resulted in a horizontal grid of 300 by 180 points. Overall computation of the 42 hours of forecast takes an average of 2 hours on 360 CPU. In these runs, Meso-NH is run coupled to ForeFireFilippi et al. (2010) code in order to provide high frequency (2 minutes) model state outputs, resulting in 252 output files containing water, temperature, cloud fraction, turbulence and U,V and W wind fields. Such high frequency outputs is an important point to, at the same time, display the complexity of local situations that can locally be very perturbed by orography and rapidly changing situations that may be critical on the field.

Still, as these forecasts cover more than one day, we focused more particularly on the prediction between T+6 h and T+30 h. The spatial resolution of the probabilistic DeepFire predictions is 640 m to reduce computational time, instead of 80 m for the deterministic predictions (cf. Section 2.3). This allows to compute an ensemble of 100 maps in a time that is about twice as long as for computing a deterministic map (presented computed duration for non-emulated maps are estimations based on a limited number of simulations, full computations were not run). For specific ignition locations, a

larger ensemble of size 10,000 is computed as well. The characteristics of both deterministic and probabilistic predictions are summarized in Table 4.

Type of prediction	Ignition points	Spatial resolution	Total number of time steps	Number of time steps in 24 hours	Ensemble members
Deterministic	1.2×10^6	80 m	253	145	1
Probabilistic	2.0×10^4	640 m	253	145	100 (10,000 locally)
Type of prediction	Total number of fire danger estimations	Computational time DeepFire, total	Computational time ForeFire, total	Computational time DeepFire, 1 forecast step	Computational time ForeFire, 1 forecast step
Deterministic	3.0×10^8	2 hours	4 months	30 seconds	half a day
Probabilistic	5.1×10^8	3.4 hours	8 months	1 minute	one day

Table 4: Characteristics of deterministic and probabilistic predictions and estimation of computational time.

The predictions are carried out and analyzed for 13 daily weather forecasts, each corresponding to the occurrence of a wildfire of 100 ha or more in Corsica island. Data on these 13 fires are available in the French database Prométhée (cf. https://www.promethee.com/, last accessed 2021.01.21) and some are reported in Table 5. Regarding the "time of fire alert" reported in Prométhée, one may assume that, before this time, the fire has ignited and started spreading and, although its size at the time is unknown, it may be close to the initial fire size of 0.45 ha assumed in DeepFire estimations. The fire size in Table 5 corresponds to the final burned surface, which results from firefighting actions and fire spread for generally more than one hour, so it does not make much sense to compare it with DeepFire predictions. Depending on the fire, the coordinates of the ignition point may be available, and in any case, its estimated location is at least identified by a square of 2 km $\times$ 2 km. When only the latter information is available, it will be

assumed that the ignition point is located at the center of the square. In either situation, the ignition point coordinates may not be perfectly accurate and one may assume that there could be an error ranging between 100 m and 1 km. For the vil_2017 fire case, the fire started on 20-10-2017 (the date indicated in Prométhée) and only spread a little then it started spreading again two days later from which it burned most of the final observed burned surface; therefore, corrected estimations of time of fire start and ignition location are reported for this fire instead of the ones available in Prométhée.

Fire id	Town	Date and time of first alert (UTC)	Fire size (ha)	Fire season
bon_05-2017	Bonifacio	30-05-2017 11h43	380.0	summer
bon_07-2017	Bonifacio	17-07-2017 11h50	121.8	summer
olm_2017	Olmeta di Tuda	24-07-2017 10h49	2118.0	summer
pal_2017	Palneca	02-08-2017 13h48	185.5	summer
cal_2017	Calenzana	05-08-2017 15h42	124.6	summer
non_2017	Nonza	10-08-2017 22h45	1617.0	summer
man_2017	Manso	11-08-2017 13h10	109.0	summer
sai_2017	Sainte Lucie de Tallano	15-08-2017 09h42	130.0	summer
vil_2017	Ville di Paraso	22-10-2017 09h00	1517.8	summer
ghi_2017	Ghisoni	26-10-2017 13h37	526.0	winter
san_2018	Saint'Andrea di Cotone	01-02-2018 04h13	1317.2	winter
chi_2018	Chiatra	03-01-2018 18h44	565.7	winter
cal_2019	Calenzana	23-02-2019 19h03	1110.2	winter

Table 5: Information on the 13 fires studied, sorted in chronological order. The "Fire id" is used to identify the fires in the present study, the one in bold being the most detailed in the following sections.

The 13 fires studied all occurred between May 2017, date from which the weather forecasts were running, and late 2019. This relatively long data

collection period ensures a relative representativeness of high fire danger meteorological conditions. Among these 13 fires, nine of them are considered to have occurred during hot, windy and dry events in the summer fire season, and the remaining four during windy events in winter fire season. In the present study, no weather forecast corresponds to a day without at least one big fire. In these situations, one may consider that fire danger was high at least at some point during the event for a fire size of at least 100 ha to be observed, especially during the summer fire season during for which more firefighting forces are mobilized to carry out the initial attack as early as possible. Availability of firefighting forces are obviously a strong factor in having a reduced burned area, a notable example being bon_05-2017, a fire happening on a low-danger day in May (no fire brigades were deployed in the territory), yet in a rather remote area so that the fire propagated freely for several hours and was barely fought.

Among those 13 fires, olm_2017, non_2017, vil_2017, chi_2018, san_2018 and cal_2019 are wind-driven fires, but with notable differences concerning the last 3 winter fires that were the result of extremely high ($>$150 km h^{-}1) wind creating intense hot and dry down slope conditions. Ghi_2017 is a different situation, with a rather high wind and dry day (not an unusual situation in autumn) but a fire started in large areas of grounded deciduous leaves that were not yet wet as no rain had fallen for a month. This created a not very intense fire, but with a lot of spotting in a mountainous area that were difficult to fight for several days. Other situations were typical of hot

dry day with some winds with less danger and resulted in smaller burned area due to the efficiency of fire fighting.

This database is yet representative of 3 years of active fire seasons with unusual, mild and severe cases, chosen thereof as a first approach to evaluate the ability to predict high danger and analyze predictions obtained using DeepFire. Although this implies that the database is somewhat biased, both winter and summer seasons are represented and the weather conditions are quite diverse from a case to another. Also, given the time range of the forecasts, there are also moments when the predicted weather conditions are less prone to fire spread.

3 Analysis of predictions for specific fires

Although IEP and DeepFire serve similar purposes, results are not directly comparable due to their different design. This section tries to tackle this issue by analyzing fire danger predictions, illustrated by figures, that address specific questions. Given the ability of the fire danger prediction system to provide very local values, we first try analyze what is the predicted fire danger in the neighborhood of the ignition location (cf. Figure 5). Then, by leveraging the high temporal resolution, we investigate how the predicted fire danger evolves over time, locally (cf. Figure 4 & 5), and for the whole simulation domain Figure 6. Using ensembles it is also possible to estimate how uncertain the prediction is (cf. Figure 8 at the ignition location and

time of fire alert, Figure 7 at the same location over time, Figure 9. and on the whole domain, cf. Figure 11, 12, 13 at the time of fire start).

Comparison with the IEP as a reference danger rating system is also of importance but not only as a pure numerical output. As being part of a differently designed system, the IEP does not address the same issues. While investigating the ability to forecast local danger, the following comparative analysis also tries to illustrate the interest of having model outputs that are both probabilistic and quantifiable in hectares.

The first part of this section illustrates this difference in designs with a detailed analysis a single case (Calenzana 2017) before a mode synthetic comparison is presented for the other 12 cases.

3.1 A detailed fire case: Calenzana 2017

Calenzana 2017 fire took place at 15h42 (UTC) on August 5th, and burned a modest 119 ha but the most part was burned in less than two hours. Figure 2 presents the meteorological situation that rapidly changed in the area, thus creating a high weather fire danger. At 12:00 a sea breeze was keeping temperatures and air relative humidity within a typical summer day, nevertheless, south-westerly winds strengthened to more than $10\,\mathrm{m\,s^{-1}}$ at 12:30, generating a down slope Foehn effect that took over the sea breeze with higher temperatures and air moisture under 30% at 13:00, which persisted up to the time of reported ignition at 15:40. The phenomenon was also observed at the nearby weather station of Calvi Airport Figure 3 although a

517 little later and more quickly than in forecast.

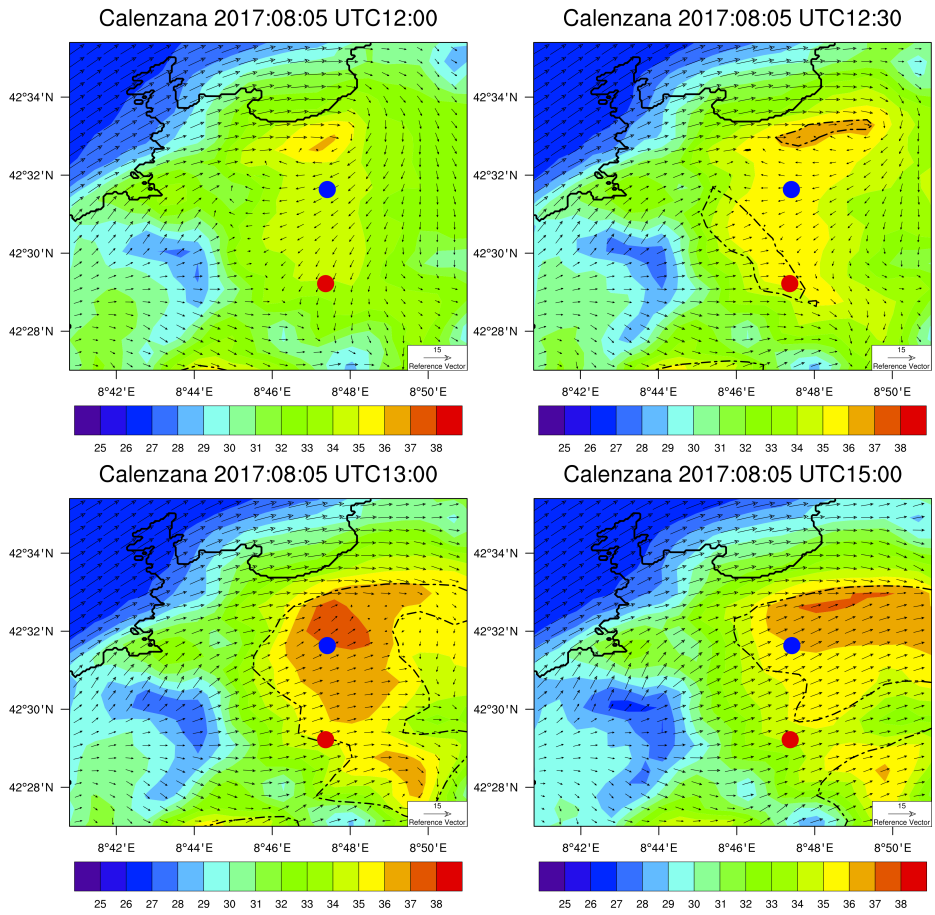

Figure 2: Model forecast at 12:00, 12:30, 13:00 and 15:00 on 08-05-2017 with surface temperature (color), wind (arrows) and area under 30% of relative humidity (dashed lines). Blue dot is the location of Calvi Airport, red dot is the fire ignition location.

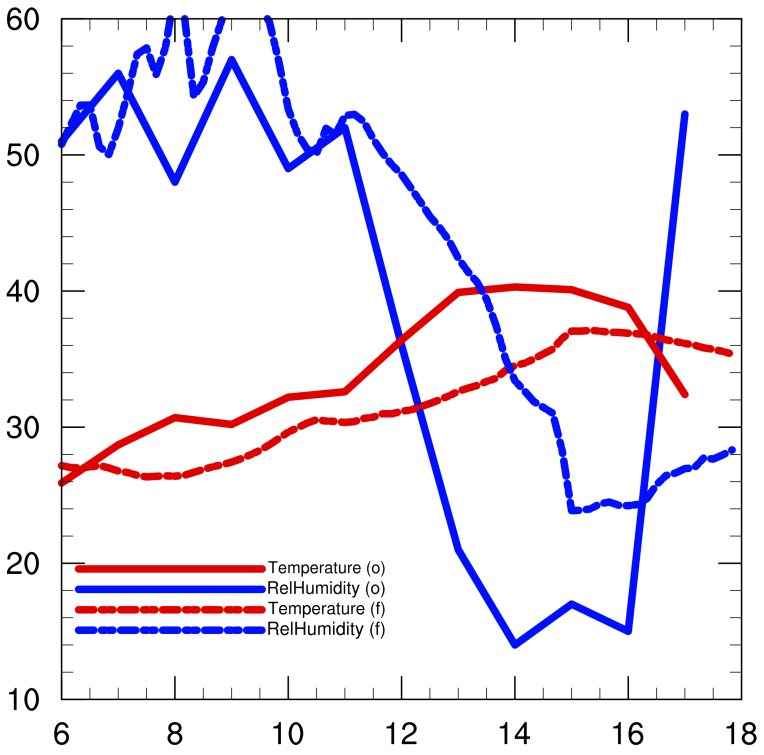

Figure 3: Relative humidity (blue) and temperature (red) observations (plain lines) and forecasts (dashed lines) at Calvi airport (blue dot in Figure 2) on 08-05-2017.

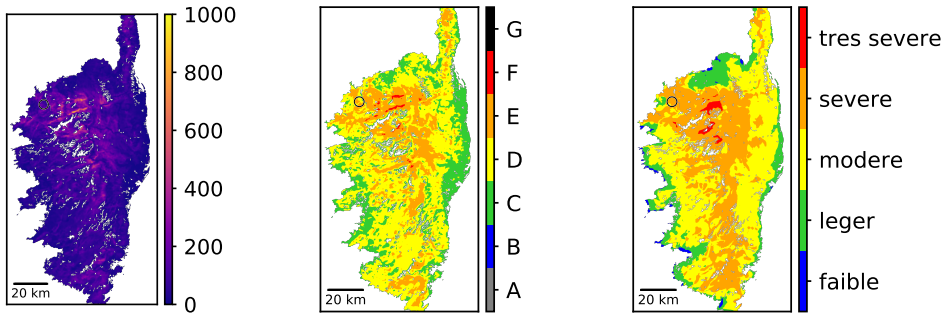

(a) DeepFire (continuous)

(b) DeepFire (categorical)

(c) IEP

Figure 4: Deterministic maps predicted based on the weather data of forecast time T+15:40 UTC (right before presumed fire start). In white are the locations that are not vegetation, where it is assumed that neither ignition nor spread is possible.
The black circle indicates the presumed location of the ignition point.

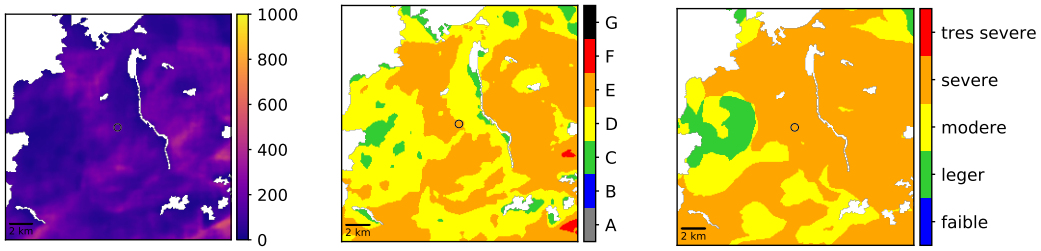

(a) DeepFire (continuous)

(b) DeepFire (categorical)

(c) IEP

Figure 5: Same as Figure 4 but zoomed around the ignition point

The deterministic fire danger maps of both DeepFire and IEP predicted at the time of fire start, are represented in Figure 4. The DeepFire value in hectares is shown in Figure 4a with a continuous color scale. The locations in white indicate the absence of vegetation, where it is assumed that neither

ignition nor spread is possible. Among the locations where fuel is present, the prediction ranges in three orders of magnitude in this specific map (from less than 1 ha to several hundreds), making it difficult to highlight the differences in fire danger with a continuous color scale. This appears more clearly with the categorical color scale in Figure 4b, where most of the island is in class D or E. Based on the correspondence between danger classes, the same can be seen on the IEP map shown in Figure 4c. Although these two maps do not perfectly match, their respective categories were determined independently, so we could expect more blatant differences. This overall similarity is probably due to the fact both indices are very sensitive to wind speed and FMC. A notable difference is that the map of IEP seems more regular than that of DeepFire. This is most likely due to the fact that the "driving" input field of IEP is the Meso-NH forecast whose original spatial resolution is 600 m, while DeepFire also accounts for a terrain field at an original spatial resolution of 80 m. Another consequence of the sensitivity of DeepFire to the terrain is more visible in Figure 5 which is zoomed around the ignition point. In Figure 5b, the ignition point is in class E, but slightly to the north-east of this point, some locations are in class D or even C. This is due to the forecasted wind in this region, which is oriented to the north-east where there is a long area from north to south with no vegetation where the fire cannot spread, hence the lower potential fire size at the aforementioned locations. In Figure 5c, it clearly appears that the IEP does not account for this characteristic, as these locations are in the same danger class as that of

the ignition point (4: “severe”).

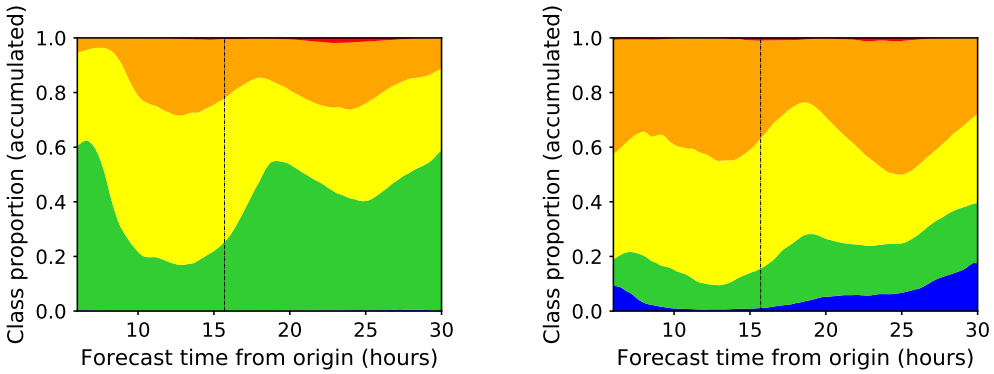

(a) DeepFire (b) IEP

Figure 6: Proportion of points on the island predicted in a given area/danger category as a function of forecast time between T+6 and T+30. The vertical line indicates the time of fire start.
(a) Categories of burned surface area range from A to G, cf. colorbar in Figure 4c.
(b) Categories of IEP range from “faible” to “très sévère”, cf. colorbar in Figure 4b.

To summarize the overall of fire danger on the island, one may compute the proportion of locations in each danger category. This “spatial” distribution is represented between T+6 and T+30 in Figure 6 for both DeepFire and IEP categories. The proportion of locations in DeepFire class E is lower than the proportion for IEP class 4 at all times, but interestingly, they increase or decrease at almost the same times. For both indices, fire danger seems to decrease on most of the island around the time of fire start, whereas the evolution of both deterministic and probabilistic DeepFire predictions at the ignition location represented in Figure 7 shows the opposite trend. At

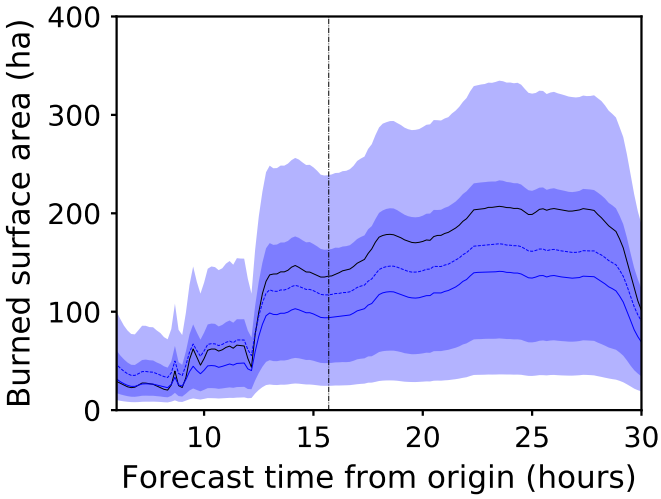

Figure 7: Ensemble of 10,000 emulated burned area (in hectares) predicted at the ignition point as a function of forecast time between T+6 and T+30. The vertical line indicates the time of fire start.
Solid black line: deterministic prediction; solid blue line: mean; dotted blue line: median.
Shaded areas delineate quantiles: first and third quartiles (dark blue); and the first and ninth deciles (light blue).

this location, the DeepFire deterministic prediction is fairly low until T+13 where an abrupt increase by about 100 ha occurs in only one hour and stays in class E until it decreases at the end of the night. This sudden increase is yet well-connected with the local conditions and the sudden increase in temperature and lower relative humidity occurring locally near the ignition area as exposed in Figure 2.

Focusing on the distribution of DeepFire values, the histogram of the probabilistic prediction obtained at the ignition location at the time of fire start is represented in Figure 8. The raw histogram is right-skewed and has a

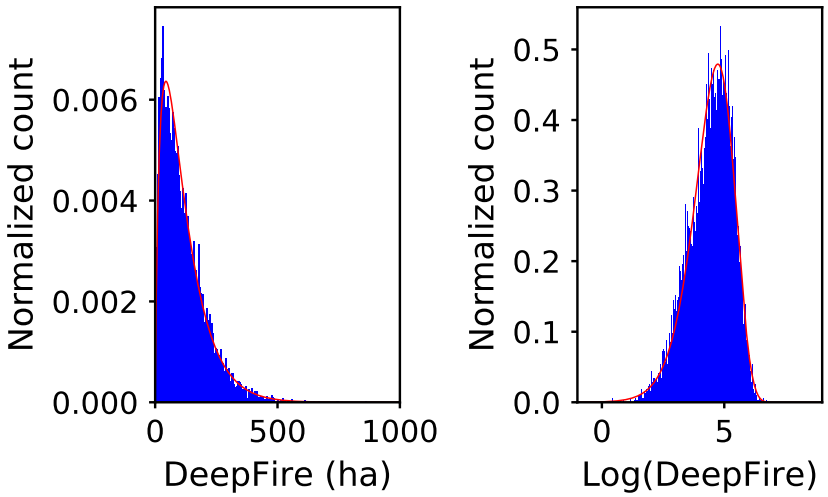

Figure 8: Distribution of the ensemble of 10,000 DeepFire values predicted at the time of fire start at the ignition location.
The red curves are the PDFs obtained from fitting the parameters of a Johnson's S_U distribution to the logarithm of DeepFire values by maximum likelihood estimation.

single mode; it may resemble a log-normal distribution at first glance, but the empirical distribution of its logarithm is fairly left-skewed instead of being symmetrical. At several other time steps and/or locations, however, a log-normal distribution fits the predicted DeepFire ensemble quite well, as shown in Figure 9a. A good agreement was obtained for most DeepFire ensembles when fitting the parameters of a Johnson's S_U distribution to the logarithm of DeepFire values by maximum likelihood estimation. This family includes normal distribution, hence the good fit in several occasions, but is also well-suited to the left-skewed distribution obtained at the ignition location and time of fire start. Still, although a Johnson's S_U distribution generally allows

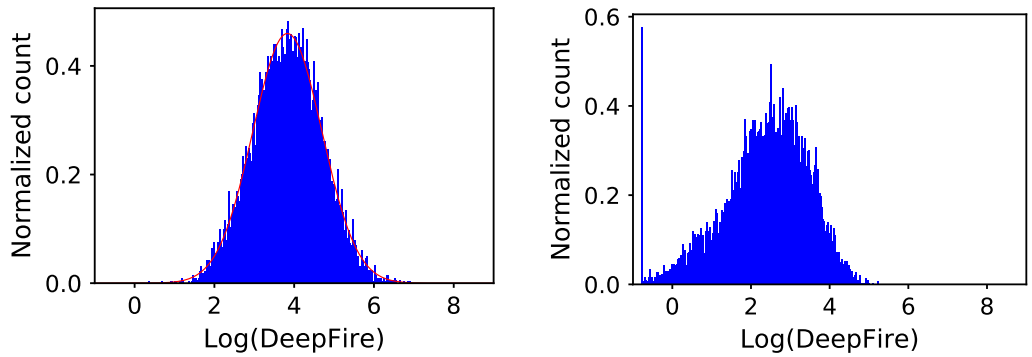

(a) Forecast time: T+18h20 (b) Forecast time: T+3h20

Figure 9: Distribution of the ensemble of 10,000 logarithm of DeepFire values predicted for the cal_2017 fire case. Contrary to Figure 8, the location is not the ignition point.
(a) The red curve is the PDF obtained from fitting the parameters of a normal distribution to the logarithm of DeepFire values by maximum likelihood estimation.

for a decent agreement, the shape of the fitted PDF associated to either the raw DeepFire value or its logarithm could match the histogram better around the PDF's mode when the distribution is skewed as in Figure 8. Also, the ensemble in Figure 9b shows that the minimum DeepFire value (0.45 ha) may be predicted for several ensemble members, resulting in a Dirac at this value that a Johnson's S_U distribution (which is continuous) cannot account for.

The distribution of DeepFire ensembles cannot be simply summarized by a simple distribution such as a log-normal. However, focusing on the ensemble mean and standard deviation reveals that over the time range of the forecast, the coefficient of variation of the DeepFire ensemble predicted at the ignition location remains between 0.7 and 1.1. For other times and/or

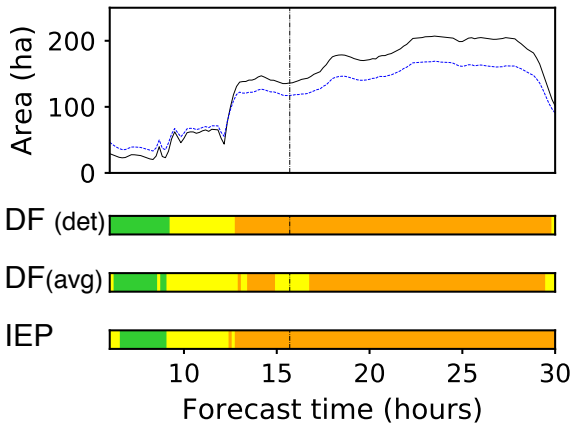

Figure 10: Predictions at the ignition point as a function of forecast time between T+6 and T+30. The vertical line indicates the time of fire start.
Top most: DeepFire both deterministic (solid black) and 10,000-size ensemble mean (dotted blue).
Horizontal colorbars, from top to bottom: category of the DeepFire deterministic area; category of the DeepFire mean area; IEP

locations, the standard deviation of the ensemble is in the same order of magnitude as its mean as well, so one may focus on the latter for simplicity. The evolution of the ensemble mean at the ignition location is represented in Figure 10 with the deterministic prediction, showing their respective fire danger categories, as well as that of the deterministic IEP for comparison. This "concise" plot reveals that the deterministic value and the ensemble mean are predicted in the same category and match with those of IEP for most of the forecast.

The probabilistic DeepFire prediction on the whole island consists in a smaller ensemble (100 members) than the local one that was analyzed previ-

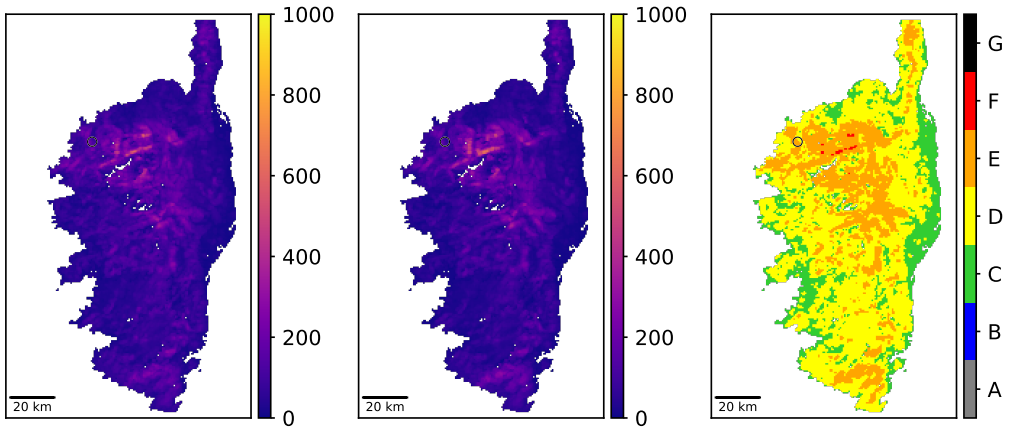

Figure 11: "Probabilistic" predicted maps at forecast time 15h40 UTC (right before fire start). From left to right: mean (continuous), standard deviation, mean (categorical).

ously (10,000 members). The ensemble of DeepFire maps predicted for the time of fire start is summarized in Figure 11 by the ensemble mean and standard deviation computed for each location. Overall, the higher the mean, the higher the standard deviation, which was also the case for the large ensemble at the ignition location. More precisely, the coefficient of variation is close to unity and for almost all locations and forecast times, it is contained in $[1/5, 5]$ in this case. Focusing on the map of ensemble mean represented with a categorical color scale, it appears similar to its deterministic counterpart represented in Figure 4b and does not provide much additional information.

In order to show the uncertainty represented by the probabilistic prediction by means of maps, one may consider other quantities than the ensemble mean and standard deviation. For instance, the fire size category with highest probability (aka, "most likely category") is computed for each location

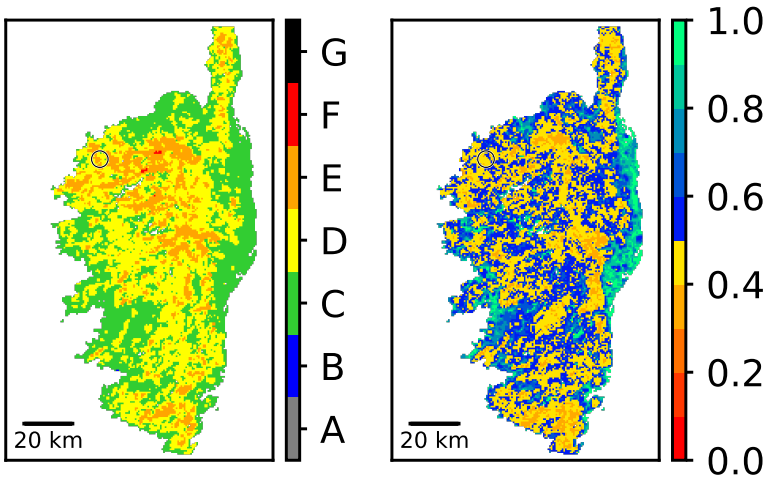

Figure 12: Most likely DeepFire size category in the ensemble (left) and associated probability (right)

and shown in Figure 12 together with the probability of this category. Like the ensemble mean, the map of most likely category is similar to its deterministic counterpart in Figure 4b. Regarding the associated probability, most locations have a probability ranging in [0.3, 0.7]. Locations whose most likely category is C tend to have probabilities closer to unity, so despite providing an intuitive representation of uncertainty, these maps do not seem to provide useful information.

Arguably, the probabilistic prediction is best represented by maps of quantiles computed for each location. Using the same quantiles as in Figure 7 as well as the ensemble minimum and maximum, the resulting map are shown in Figure 13. These maps can be understood as predicted scenarios that range from most optimistic (ensemble minimum at the left) to most

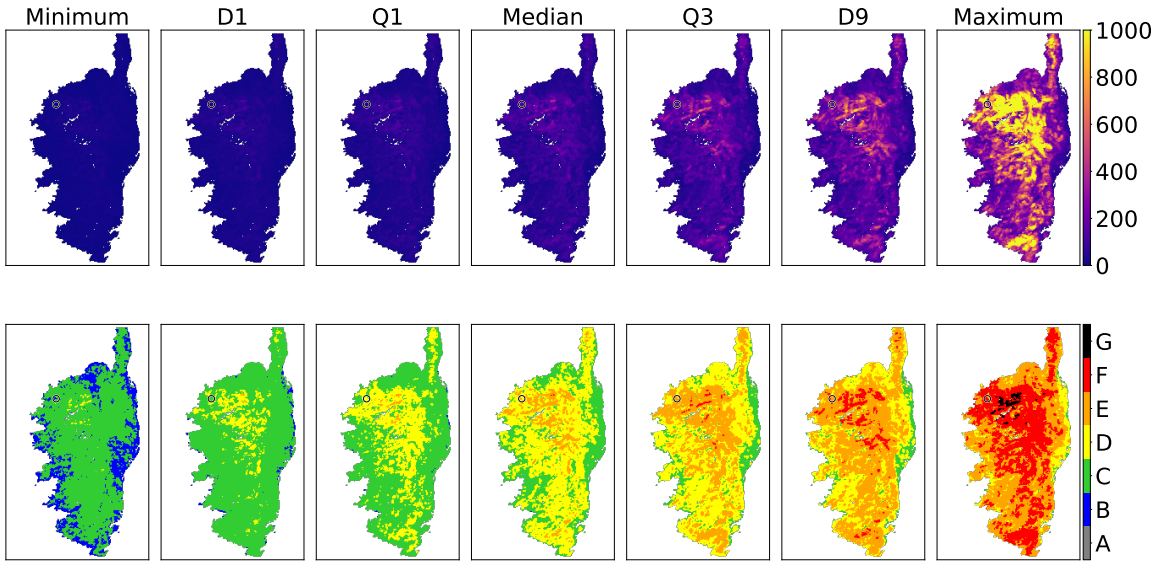

Figure 13: Statistics of the ensemble of DeepFire values predicted for the time of ignition mapped over Corsica island (Calenzana 2017.08.05)
Upper row: continuous; lower row: categorical
Q1 and Q3: first and third quartiles; D1 and D9: first and ninth deciles.

pessimistic (ensemble maximum at the right). It is arguably a more intuitive way to represent the uncertainty in the prediction than with the standard deviation or the probability of the most likely category. In this case, it seems that the map of minimum and, to some extent, the map of first decile show scenarios where fire danger categories are underestimated. Likewise, the map of maximum overestimates fire danger, but the other maps where fire danger is not as extreme seem fairly relevant.

3.2 Overview of predictions for all 13 fires

The fire danger predictions for fire case cal_2017 that were presented in detail in Section 3.1 were also carried out for the 12 other fire cases listed in Table 5.The present section summarizes results for all 13 fire cases.

Fire id	IEP	DeepFire (ha)	Mean (ha)	[Q1, Q3] (ha)	$\mathbb{P}$[B]	$\mathbb{P}$[C]	$\mathbb{P}$[D]	$\mathbb{P}$[E]	$\mathbb{P}$[F]	$\mathbb{P}$[G]
bon_05-2017	3	72.6 (D)	67.2 (D)	[26.3, 86.2]	0.008	0.397	**0.464**	0.127	0.004	0
bon_07-2017	4	159.8 (E)	143.0 (E)	[60.5, 193.3]	0	0.126	**0.422**	0.415	0.037	0
olm_2017	4	368.3 (E)	272.5 (E)	[103.3, 362.5]	0	0.048	0.260	**0.478**	0.214	0.001
pal_2017	4	194.8 (E)	137.0 (E)	[54.5, 159.8]	0	0.139	**0.489**	0.324	0.048	$< 10^{-3}$
cal_2017	4	136.0 (E)	117.1 (D)	[47.8, 163.1]	$< 10^{-3}$	0.207	**0.403**	0.377	0.012	0
non_2017	3	118.9 (D)	106.7 (D)	[35.3, 130.8]	0.001	0.292	**0.433**	0.246	0.028	0
man_2017	2	38.7 (C)	27.9 (C)	[3.45, 32.8]	0.268	**0.531**	0.163	0.037	0.002	0
sai_2017	4	71.7 (D)	66.7 (D)	[25.3, 83.2]	$< 10^{-3}$	**0.439**	0.431	0.126	0.004	0
vil_2017	4	453.6 (F)	309.6 (E)	[59.6, 370.5]	$< 10^{-3}$	0.167	0.263	**0.344**	0.213	0.013
ghi_2017	3	55.9 (D)	63.6 (D)	[32.1, 77.6]	0	0.384	**0.518**	0.097	0.001	0
san_2018	3	172.3 (E)	144.2 (E)	[49.6, 182.1]	0.003	0.198	0.369	**0.378**	0.052	$< 10^{-3}$
chi_2018	4	483.0 (F)	312.5 (E)	[79.1, 405.6]	0	0.099	0.272	**0.378**	0.245	0.005
cal_2019	5	431.9 (F)	450.1 (F)	[181.5, 578.9]	0	0.007	0.121	**0.467**	0.395	0.010

Table 6: Summary of the fire danger predictions on all 13 fire cases at the presumed location of fire start.
Q1 and Q3: first and third quantiles.
$\mathbb{P}$[X]: predicted probability of being into class X of burned surface area; in bold is the highest probability among all 6 classes.

The deterministic predictions of IEP and DeepFire at the ignition location and time of fire start for each fire are listed in Table 6, together with some statistics of the associated ensemble of 10,000 DeepFire predictions. The DeepFire ensemble mean is generally a bit lower than the deterministic value, except for two fires (ghi_2017 and cal_2019). Both ensemble mean and

deterministic value are generally slightly lower than the ensemble's third quantile, except for man_2017 fire where the deterministic value is slightly higher. In terms of fire size categories, whether we consider the deterministic DeepFire value or the ensemble mean, the most likely category is either the same or one level lower. The most likely category is either C, D, or E, and in almost all cases, probabilities of being in category B and G are very low. Comparing the deterministic predictions of IEP and DeepFire, there is an agreement between fire danger categories for 9 out of 13 cases. Due to the categorical nature of these ratings, difference of one category are expected and require a more detailed analysis proposed thereafter.

Fire id	B	C	D	E	F	G	1	2	3	4	5	E+	4+
bon_05-2017	4.6%	39.0%	**52.0%**	4.3%	< 0.01%	0%	32.1%	**40.5%**	23.1%	4.3%	0%	4.3%	4.3%
bon_07-2017	< 0.01%	10.0%	**52.8%**	37.0%	0.2%	0%	0.1%	3.3%	33.0%	**63.3%**	0.2%	37.2%	63.5%
olm_2017	5.1%	13.3%	39.7%	**40.6%**	1.3%	0%	9.1%	22.4%	**39.8%**	28.4%	0.3%	41.9%	28.7%
pal_2017	< 0.001%	13.1%	**47.5%**	38.9%	0.5%	0%	< 0.1%	2.1%	18.3%	**76.1%**	3.4%	39.4%	79.5%
cal_2017	< 0.01%	25.2%	**52.6%**	21.7%	0.5%	0%	1.1%	14.4%	**47.5%**	36.0%	1.0%	22.5%	37.0%
non_2017	0.8%	29.9%	**34.5%**	33.2%	1.6%	0%	14.2%	28.8%	**33.9%**	22.3%	0.8%	34.8%	23.1%
man_2017	7.9%	8.4%	32.1%	**46.2%**	5.4%	0%	8.8%	14.8%	**41.8%**	31.6%	3.0%	51.6%	34.6%
sai_2017	< 0.01%	23.6%	**67.8%**	8.7%	< 0.001%	0%	0%	5.6%	**64.5%**	29.9%	0%	8.7%	29.9%
vil_2017	28.6%	17.4%	**33.1%**	18.8%	2.0%	0%	**36.4%**	31.2%	26.7%	5.6%	< 0.1%	20.8%	5.6%
ghi_2017	< 0.01%	41.8%	**52.6%**	5.6%	0%	0%	4.9%	32.0%	**53.3%**	9.8%	0%	5.6%	9.8%
san_2018	**38.4%**	11.6%	27.7%	22.3%	< 0.1%	0%	**43.4%**	39.6%	15.6%	1.5%	0%	22.3%	1.5%
chi_2018	**35.0%**	6.7%	16.4%	32.8%	9.0%	0%	26.4%	**36.4%**	18.4%	15.0%	3.8%	41.8%	18.8%
cal_2019	1.1%	9.7%	31.2%	**43.2%**	14.8%	< 0.1%	1.6%	4.9%	19.6%	**55.6%**	18.2%	58.0%	73.8%

Table 7: Summary of the fire danger predictions on all 13 fire cases over the whole island at the time of fire start: proportion of each class for both DeepFire (B to G) and IEP (1 to 5). In bold is the highest proportion among all classes.
Last two columns: proportion of locations in DeepFire class E or higher (E+) and proportion in IEP class 4 or higher (4+).

Focusing on deterministic prediction at the time of fire start for each fire, the maps of both DeepFire and IEP are summarized in Table 7 by the proportions of locations on the island predicted in either category of both fire danger indices. In all fire cases, the proportion of the island that is in class G is null or quasi-null and in most cases, the respective proportions of class F and class 5 are also quite low. Proportion of class B is low in many cases too, but there are 3 of them where it is higher than 25% because a non-negligible part of the island is predicted with a FMC higher than 0.3. This, together with the predicted probabilities listed in Table 6 reveals a limit of using the fire size classes of the US system to quantify fire danger with DeepFire. The thresholds of class B and G are very restrictive (upper bound of 4 ha and lower bound of about 2000 ha, respectively) considering that DeepFire estimates the potential fire size of a fire that spreads freely during one hour. The same holds to some extent for class F (lower bound of about 400 ha), explaining the lower representativeness of the extreme classes in most cases.

Among the 13 cases, the fire danger category that has the highest proportion is generally class D for DeepFire and 3 for IEP. Comparison with the local deterministic predictions in Table 6 reveals that, in almost all cases, the deterministic prediction is in equal or higher danger class than the category with the highest proportion over the island for both IEP and DeepFire, the only exception being man_2017 fire case. This means that using either index, the ignition point belongs to the areas that are “highlighted” at the time

of fire start, which is a desirable property of a fire danger map. It would be even better to observe the same property at the sub-regional scale because the environmental conditions and values at stake can be quite different from one to another, and make more sense from an operational perspective than the average over the island.

The previous tables provide data regarding the prediction at the time of fire start, but the evolution of fire danger over time needs to be assessed as well. For simplicity, we decided to present only two of the figures that were shown in the previous section regarding cal_2017 fire case, for the 12 other cases. The zoom around ignition point of the DeepFire deterministic map at the time of fire start with categorical color scale (cf. Figure 5c) provides a prediction of fire danger at the sub-regional scale, while the "concise" plot in Figure 10 shows the evolution at the ignition point of the deterministic DeepFire prediction, the ensemble mean, and the IEP. These two figures are shown for the 12 fire cases in Figure 14. Similarly to the cal_2017 fire case, lower DeepFire values are obtained close to areas with no vegetation that block fire spread in several instances, but this mainly depends on the direction of wind speed.

In the case of bon_07-2017 for instance, the wind comes from the east, so when getting closer to areas without vegetation, lower values (classes D and C) are obtained to the west of the ignition location, but higher values (class E) are obtained eastward. Regarding the DeepFire predictions over time at the ignition location, the deterministic value and the ensemble mean

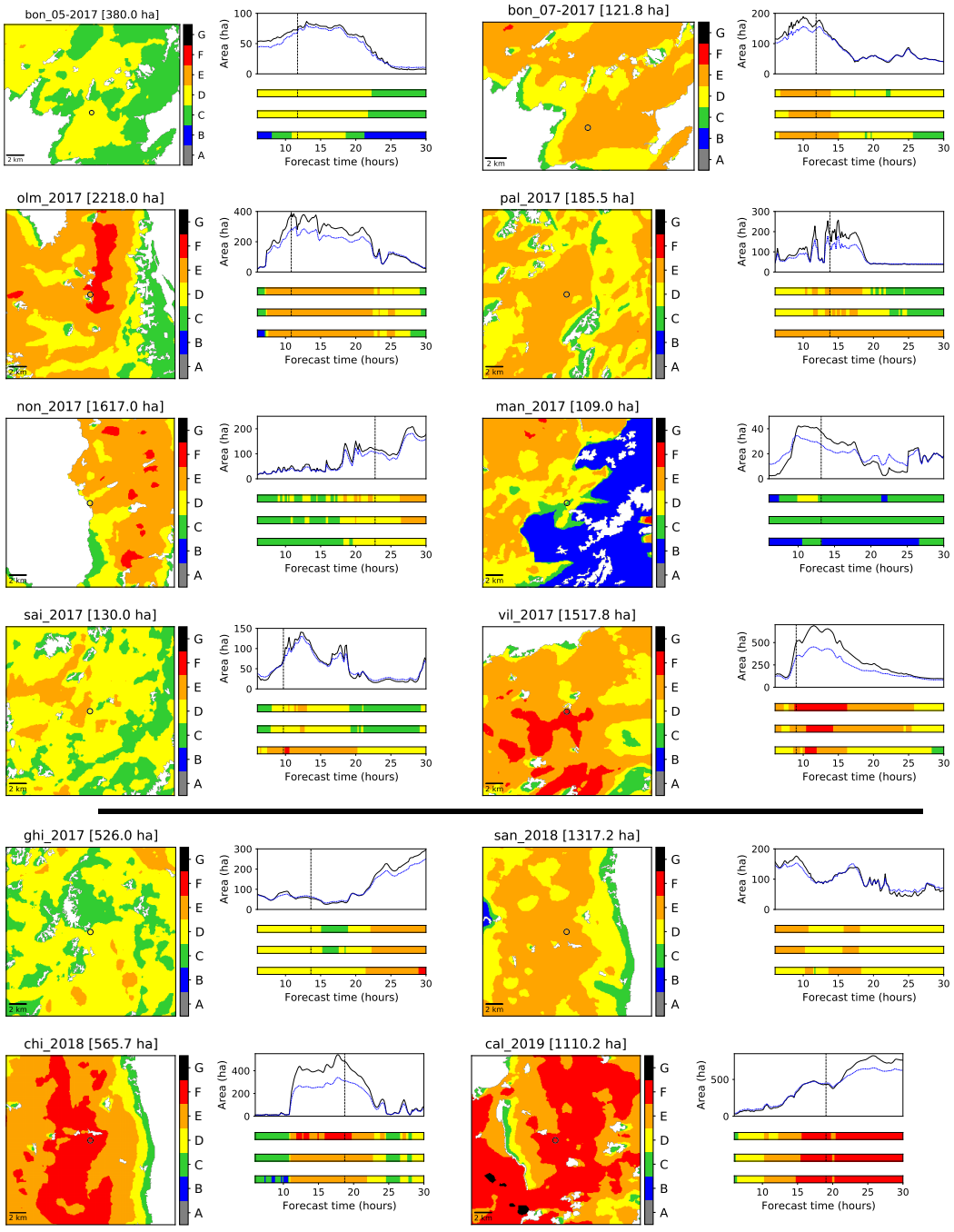

Figure 14: For all 12 complementary fire cases: map of DeepFire predicted at the ignition time zoomed around the ignition location (left, cf. Figure 5c), as well as the "concise" plot for the ignition location (right, cf. Figure 10). Eight top-most: summer fires; four bottom-most: winter fires.

are generally close and in the same fire danger category. The ensemble mean seems to follow the same variations with equal or lower magnitude, resulting in predictions in a smaller ranger than its deterministic counterpart, especially when the latter is very high (> 200 ha). The category of IEP generally matches that of DeepFire, but can be higher or lower by one level for a few hours. There is a notable exception for Sainte Lucie de Tallano where IEP is in the highest class (5) while DeepFire is in class D (2 levels lower), but it can be observed as well that area nearby is only 1 level under (class E).

Looking at the DeepFire deterministic prediction more globally, one may notice that close to the ignition point and/or in a few hours after fire start, higher fire danger classes can be obtained. Five fire cases are concerned: olm_2017 (eastward), non_2017 (eastward and about five hours after fire start), man_2017 (to the north-west), sai_2017 (eastward and after about two hours), and ghi_2017 (about eight hours after fire start). Therefore, considering the vicinity of the ignition point and/or a few hours after fire start, class E or higher is predicted in most cases. This does not happen in two cases: ghi_2017 (class D) where the fire burned slowly and several fire starts occurred, and bon_05-2017 (class D), whose observed fire size (109 ha) is the smallest among the 13 fires studied.

It may make more sense to focus on local predictions in time and space to evaluate predictions of ignition, but DeepFire estimates potential fire spread, so it should be analyzed over a larger range in time and space. For instance, some fires such as non_2017 may spread slowly at first, yet become difficult to

stop after some time due to a change in weather conditions and/or when they reach locations with high slope or specific fuel type that are more favorable to fire spread.

4 Possible designs for daily fire danger mapping

Focusing on the vicinity of the ignition location and the few hours after fire start, the DeepFire predictions proved to be satisfactory. However, in practice, information on the fires used in the previous section is not known before making fire danger predictions. For the fire cases studied, we knew what were the areas and times to focus on because the information was known *a posteriori*. One could analyze the maps predicted for each time step, but in an operational context one or a few maps that summarize the daily predictions of fire danger. In the present section, we propose several ways of summarizing the predicted fire danger maps and discuss how relevant the resulting daily maps could be in an operational context.

The maps proposed in the present section attempt to address several questions. First, what are the locations and time where/when fire danger is highest for the day to come? (cf. deterministic: Figure 15 & 16, and probabilistic: Figure 17 & 18) Then, starting from when and for how long is there high fire danger? (cf. Figure 19 and Figure 20.) Regarding these aspects, the question of uncertainty in the prediction is also addressed to some extent

by comparing the deterministic maps to their probabilistic counterparts.

Similarly to Section 3, several maps are first proposed and detailed for cal_2017 fire case, then a summarized analysis is provided for all 13 fire cases.

4.1 Focus on the day of Calenzana 2017 fire

From the deterministic prediction of either DeepFire or IEP, the maximum over the day can be computed easily for each location. The maps of the maximum between T+6 and T+30 of DeepFire (resp., IEP) and of the associated time of maximum are shown in Figure 15 (resp., Figure 16). On this fire day, relatively strong south-westerly wind was definitely the driving factor, but this wind also brought some humidity, leaving area of high danger either where a downslope effect was strong. By looking at the time of the maximum of DeepFire on the right of Figure 15 it can be seen that although there is a high danger potential (some areas in red in map on the left), there is actually much contrast regarding time of highest danger in the area of Calvi, suggesting that if there is an event, a detailed local analysis is required. On the IEP map in Figure 16 such requirement is less obvious, with large areas marked in orange and less contrast, indicating a dangerous but more general situation (less discriminant) with an event having strong probabilities of occurring in the morning.

If the maximum is obtained at several forecast times, we show the earliest one. Because the IEP has only 5 categories, the maximum value will

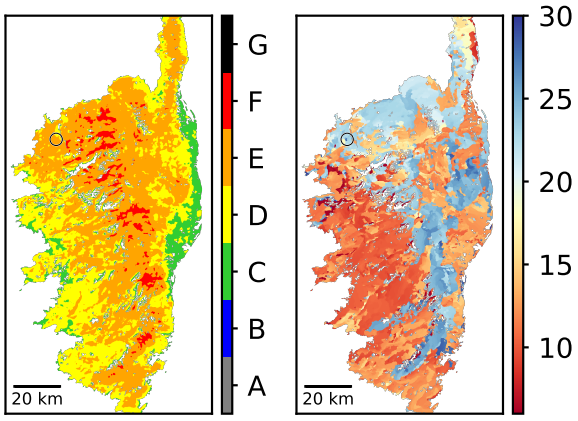

Figure 15: Maximum over the forecast between T+6 and T+30 (left) and time thereof (right) of the DeepFire prediction.

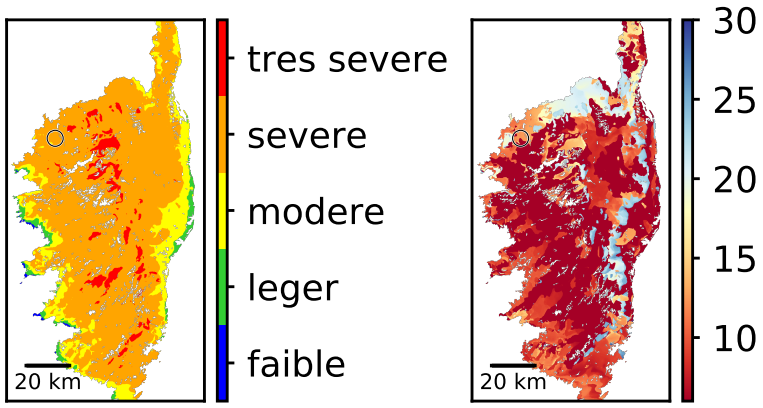

Figure 16: Same as Figure 15 but for IEP prediction

most likely be predicted at several times. Figure 16 shows that the time of maximum is T+6 for most locations, making it hard to tell when fire danger is highest. In practice, this issue can be avoided by identifying the time of maximum of another a continuous quantity, such as the FFMC which is one of the two components of IEP. In Figure 15, although the maximum is rep-

resented by a categorical color scale, it corresponds to a continuous index, so this issue does not occur. The time of maximum for DeepFire predictions is between T+8 and T+18 on the majority of the island, but for some locations (even among these predicted in class F) the time of maximum is after T+18, notably around the ignition location where the fire occurred at T+16 while the maximum is more around T+22.

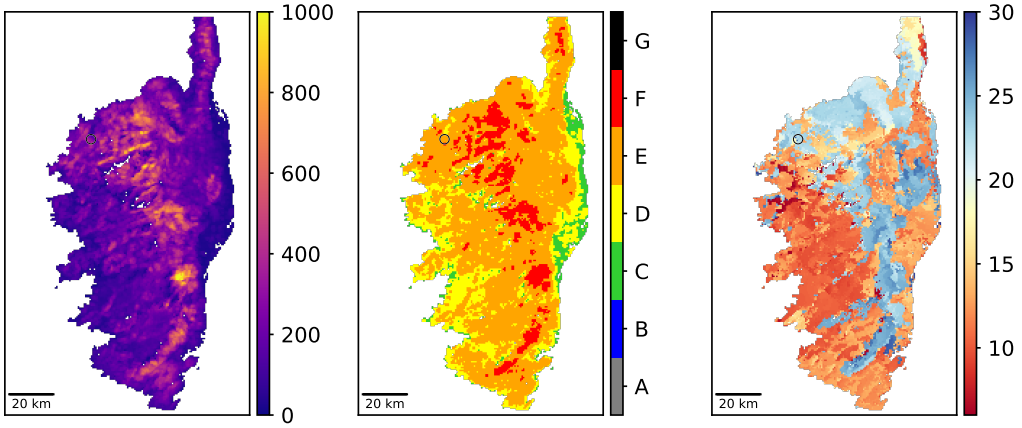

Figure 17: Maximum over the forecast between T+6 and T+30 of the quantile for probability 0.8 in the ensemble of DeepFire predictions.
From left to right: continuous scale; categorical scale; time of the maximum.

From the probabilistic forecast of DeepFire, the computation of a counterpart to Figure 15 is less direct. The ensemble can be summarized by a statistic such as the mean or a quantile. For either statistic, it makes more sense to first compute it for all locations and forecast times, then to identify the time of maximum. In the case of a quantile, for instance, the time of maximum can therefore be interpreted to that of a more or less optimistic predicted scenario. In Figure 17, the quantile for probability 0.8 was chosen.

According to the Prométhée database, about 80% of the fires in Corsica have a final burned surface of 1 ha or less, which is quite low considering the range of DeepFire predictions. Although it is intuitive to define quantile from a meaningful fire size derived from a database of observations, it does not seem relevant here, and it makes more sense to interpret the chosen quantile as a quantity that represents a quite "pessimistic" scenario, yet not too extreme given the previous analysis of Figure 13. However, as can be seen in Figure 17 (middle map) there are still many locations where fire danger is at least in class D. It might be possible to make a distinction among the high-danger areas by looking at the continuous value (left map) less intuitive. Regarding the time of maximum, it is similar to that of the deterministic counterpart in Figure 15.

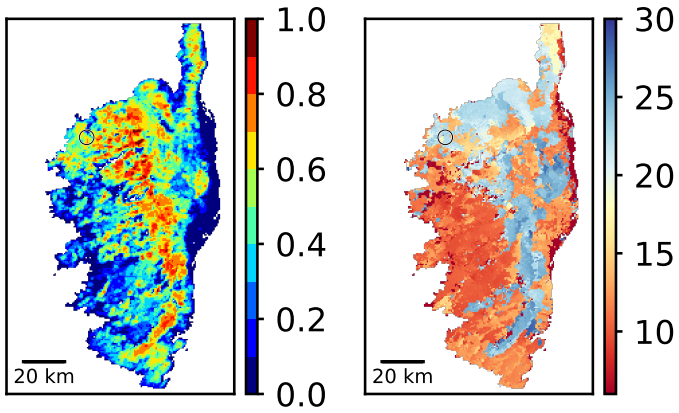

Figure 18: Maximum over the forecast between T+6 and T+30 of the probability of being into class E or higher (left) and time thereof (right).

Alternatively, one may consider another maximum over time: that of the

probability (based on the ensemble) of being into class E or higher. The resulting map for cal_2017 fire case is shown in Figure 18 together with the associated time of maximum. Compared to Figure 17, the maximum probability seems better suited to discriminate among locations with high fire danger during the day, whereas the time of maximum appears similar overall, except for some locations where the predicted probability is 0 over all 24 hours, resulting in a time of maximum at the value of T+6 by default.

Among all the maps presented in the present section up to this point, the maps of time of maximum to point out that the evolution of fire danger over time does not necessarily result in a peak at a single given time (e.g., midday) everywhere. Still, the time of maximum fire danger might not be the most relevant information for daily predictions as there can be high fire danger for an extended period of time.

Regarding the evolution of DeepFire predictions during the day, a more relevant quantity could be the earliest time of being into class E or higher if it happens at all. The associated maps resulting from the deterministic and probabilistic predictions are represented in Figure 19. In the case of the probabilistic version, the earliest time when class E is predicted may differ from a member of the ensemble to another and the class may not be reached for some of them, so the conditional mean among the sub-ensemble of members for which the class is reached is provided. According to the deterministic version in Figure 19a, there is about a quarter of the island where class E is never reached. However, according to its probabilistic counterpart in Fig-

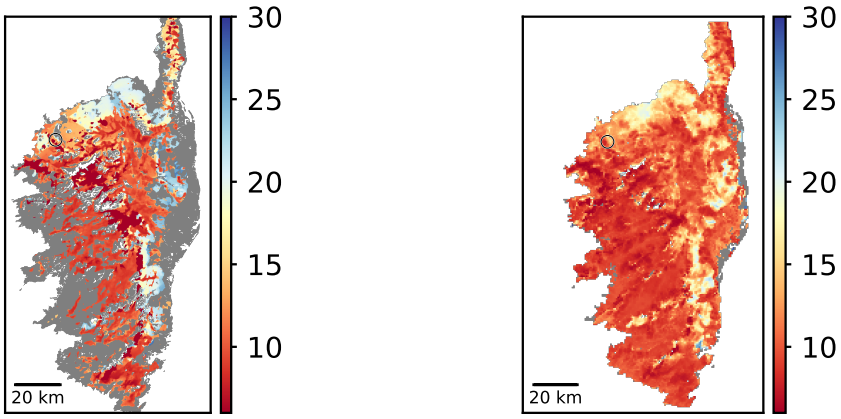

(a) Deterministic (b) Probabilistic

Figure 19: Earliest time between T+6 and T+30 of a location being predicted into class E or higher (in gray if it does not happen).
The probabilistic version is the conditional mean among the ensemble of the time when class E is reached on the condition that it is reached (a gray area is shown otherwise)

ure 19b, almost all locations have at least one member in the ensemble for which class E is predicted at some point (but the amount of these members may differ between locations), and the map is more homogeneous with fewer extreme values.

To complete the information provided by the previous maps, one may compute the total duration between T+6 and T+30 when a given location has a DeepFire prediction of class E or higher. In the case of the probabilistic prediction, there is no need to consider a conditional mean as the duration is null if class E is never reached. The deterministic version is shown in Figure 20a, while both mean and standard deviation of the ensemble are shown in Figure 20b to represent the probabilistic forecast. Once again, the map of

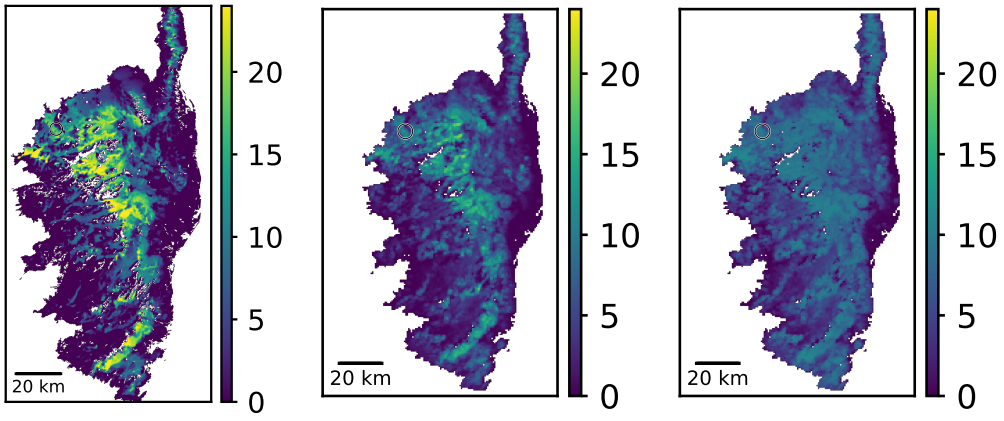

(a) Deterministic (b) Probabilistic prediction

Figure 20: Total duration a location is predicted in class E or higher over the forecast between T+6 and T+30. The colorbar indicates the duration in hours.
(b) Mean (left) and standard deviation (right).

ensemble mean is more homogeneous than its deterministic counterpart and the standard deviation seems higher in locations where the mean is higher.

The analysis of cal_2017 fire case reveals that predicted time of maximum fire danger is similar even when the input uncertainty is accounted for using the calibrated distribution. However, based on the calibrated distribution, the predicted duration of high fire danger is quite uncertain. Such quantity may not serve as a daily fire danger index, but it appears interesting as a complement, because the longer high fire danger conditions last, the more severe the situation may be considered, even if the maximum fire danger category over the day is the same. Still, in the case of DeepFire predictions, not only is the prediction uncertain, but it is also quite sensitive to the choice

of the fire size threshold used to define high fire danger categories.

4.2 Overview of the predictions for the 12 other fires

A number of numerical quantities that could serve as a daily indicator were proposed. Due to its ability to discriminate between locations with high fire danger in the cal_2017 fire case, the maximum over the forecast between T+6 and T+30 of the probability of being into class E or higher is chosen as a daily fire danger map for the 12 other fire cases. This map is shown for all 12 cases in Figure 21, together with the evolution of the proportion in the island of each class for both DeepFire and IEP according to the deterministic prediction (cf. Figure 6) to have an idea of how the overall spatial distribution of fire danger evolves over time.

Overall there is a general agreement in variations between T+6 and T+30 between IEP and DeepFire, with a general trend of more "contrasted" DeepFire predictions, indicating a better ability to pinpoint high danger locations (i.e. it is more discriminant).

As in Section 3.2, one could present some scalar results regarding the overall spatial distribution of fire danger over time, but considering an average in time and space does not reflect the variations of fire danger and, therefore, does not seem very relevant. Arguably, a daily rating of fire danger based on DeepFire should be computed on a relatively large area, at the sub-regional level for Corsica island and the maximum value over the day can be considered. At this spatial scale, a representative fire danger rating could

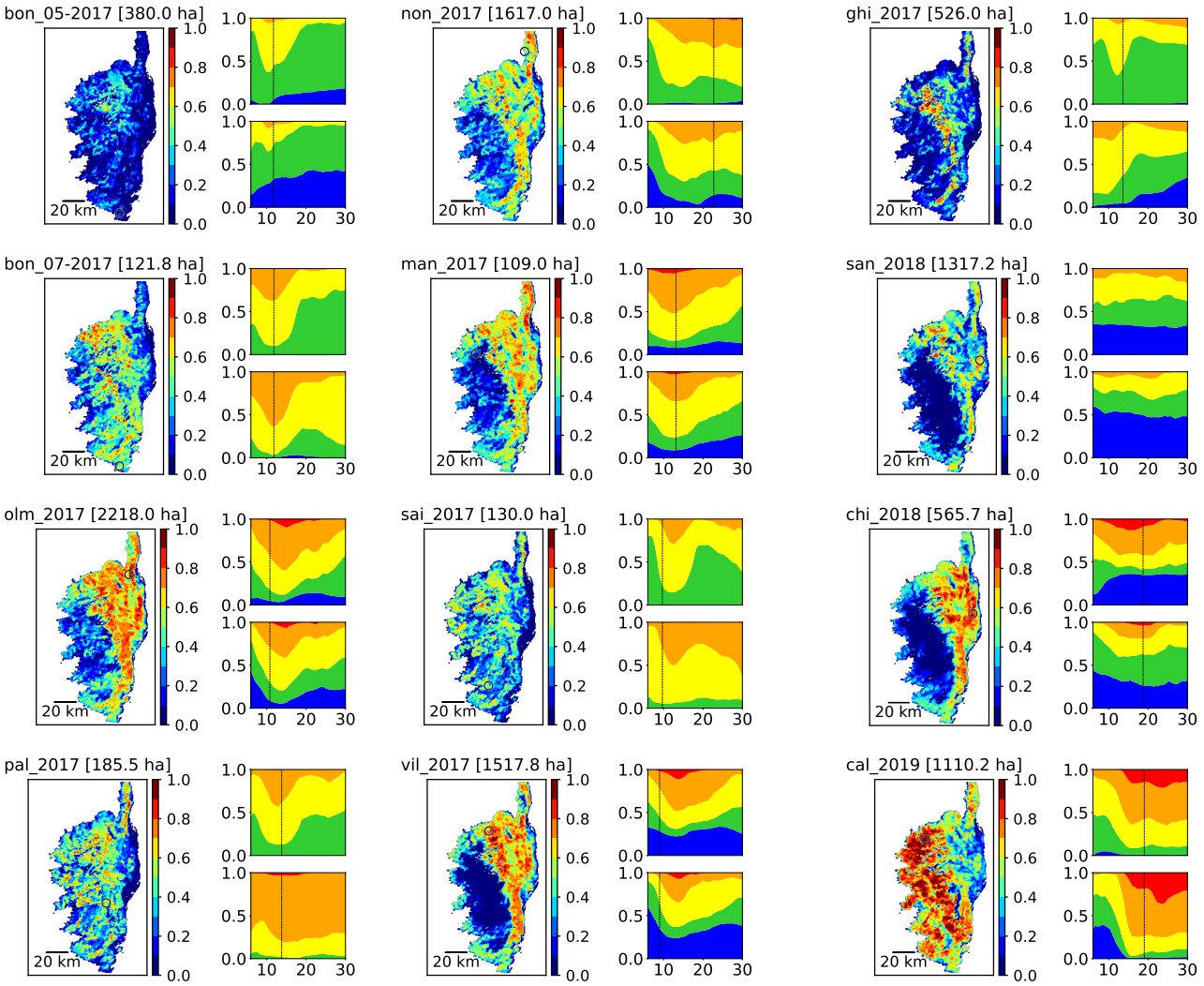

Figure 21: For all 12 complementary fire cases: maximum between T+6 and T+30 of the probability of being into class E or higher (left, cf. Figure 18), together with the evolution of the proportions over the island of DeepFire (top right, cf. Figure 6a) and IEP (bottom right, cf. Figure 6b) classes. First two columns: summer fires; last column: winter fires.

be the one associated to the DeepFire value that separates the 80% lower values from the 20% highest in a given area. As a complement to fire danger ratings, that are associated to a low spatial resolution, it makes sense to use the predictions with high spatial resolution and high frequency to analyze the situation in more detail.

5 Conclusions and perspectives

We have shown a new method to compute fire danger predictions by estimating a potential fire size using the deep neural network DeepFire in a reasonable computational time. This allows for the generation of a sequence of high resolution maps of fire danger with high frequency, and an ensemble of such predictions that account for input uncertainty, although at lower spatial resolution. Several quantities derived from predictions of potential fire size can be computed such as maximum fire danger over time, duration of high fire danger, and probabilistic versions thereof using the ensemble. Analysis of the predictions on 13 fire cases showed that, overall, DeepFire predicts higher fire danger in the neighborhood of the ignition location and around the time of fire start. The temporal variation over the day make it difficult to summarize the predictions by a few daily fire danger indices. A few quantities were proposed to serve the purpose of providing a daily indicator, but the evolution in time, the granularity, and the uncertainty of the predictions can provide useful information to a forecaster. It is also important to note

that all these computations were actually run in a batch processing mode to ensures its potential to run in an operational context.

A major strength of the prediction using DeepFire seems to be its spatial granularity allowing to be more discriminant. Compared to traditional fire danger indices that mostly rely on weather forecasts, the potential fire size estimated by DeepFire accounts for the influence of terrain on fire spread at via the variability over space in type of vegetation, presence of non-burnable areas, and slope. The high-resolution maps could be used as complement of fire danger ratings, that generally attribute a single value to a large area, for better anticipation but potentially to help to decide firefighting actions after a fire has started spreading. For instance, the maps can be used to finely identify locations that, if reached at a some point, the fire will spread even faster and become harder to control. Moreover, another strength regarding its design, compared to other fire danger rating systems, is that it is not based on empirical knowledge, except for the actual choices of fire size for each class, these results are not based on experience of past fires, nor on expert analysis.

The present study allowed identifying several aspects that could be investigated further or improved. Regarding the DeepFire ensemble at a given time and location, it seems that the logarithm follows a Johnson's S_U distribution in several instances, although a more complex family of distribution could lead to a better fit in more instances. Statistical inference of the ensembles could also be analyzed at a larger scale, by considering several forecast

times and locations, and even the predictions for several days. The analysis of the distribution of numerous potential fire sized predicted by DeepFire could lead to the definition of meaningful thresholds to define categories of fire danger that are better suited than the US classifications which pertains to all observed fires. Defining the thresholds based on observed fire sizes appears difficult in Corsica where a vast majority of fires are attacked early enough to spread far, even when fire danger is high.

Information on the intermediate sizes of the fires, rather than that of the final burned surface, would be more relevant for comparison with DeepFire, but is difficult to measure. If DeepFire predictions were to be used in operational conditions, the feedback would be very valuable to adjust the thresholds, but also to evaluate the usefulness of such a prediction system. Regarding uncertainty, only a deterministic weather forecasts were used, but probabilistic weather forecasts could be used as an alternative or as a complement to represent the probabilistic distribution of wind and FMC inputs of DeepFire.

DeepFire focuses on wildfire spread, and could be associated to predictions representing ignition probability for a better estimation of fire danger. A model of ignition probability should account at least for weather predictions, and other data sources such as proximity to roads or cities could be included to design such a model, which would result in a distribution that is not uniform among burnable locations. Ignition probability is also a major component of wildfire risk quantification frameworks, where DeepFire could

be used to estimate fire spread. Although the computational time constraints of fire risk assessment are not as tight as for those of daily fire danger predictions, DeepFire could estimate a very large number of potential fire sizes in a reasonable amount of time, much larger than it would be using traditional fire spread simulators, allowing for better and/or more detailed risk quantification. For a complete assessment of risk, however, the values at stake are not just hectares of land burned and should be accounted for more explicitly than with DeepFire. A step in this direction could therefore be to train a DNN in a similar fashion as DeepFire but based on an estimated cost.

Whether it be for fire danger or risk, DeepFire predictions should be also considered and evaluated over a long time period (e.g. a whole year) that includes both days with and without fires occurrence. Due to their ability to account for several types of data, and to carry out fast computations, deep neural networks appear promising to address the complexity of wildfires and design better prediction systems.

Acknowledgments

Funding: This work was supported by the Agence Nationale de la Recherche, France [grant number ANR-16-CE04-0006 FIRECASTER].

Conflicts of interes

The authors declare no conflicts of interest.

References

Allaire, F., Filippi, J.-B., and Mallet, V. (2020). Generation and evaluation of an ensemble of wildland fire simulations. *International Journal of Wildland Fire*, 29(2):160–173.

Allaire, F., Mallet, V., and Filippi, J. B. (2021a). Emulation of wildland fire spread simulation using deep learning. preprint.

Allaire, F., Mallet, V., and Filippi, J.-B. (2021b). Novel method for a posteriori uncertainty quantification in wildland fire spread simulation. *Applied Mathematical Modelling*, 90:527–546.

Amodei, M., Isabelle, S., and Stein, J. (2015). Verification of the french operational high-resolution model arome with the regional brier probability score. *Meteorological Applications*, 22.

Bradshaw, L. S., Deeming, J. E., Burgan, R. E., and Cohen, J. D. (1984). The 1978 national fire-danger rating system: technical documentation. Gen. Tech. Rep. INT-169. Ogden, UT: U.S. Department of Agriculture, Forest Service, Intermountain Forest and Range Experiment Station. 44 pp.

Burgan, R. E., Andrews, P. L., Bradshaw, L. S., Chase, C. H., Hartford,

R. A., and Latham, D. J. (1997). Current status of the wildland fire assessment system (wfas). *Fire Management Notes*, 57(2):14–17.

Filippi, J.-B., Morandini, F., Balbi, J. H., and Hill, D. R. (2010). Discrete event front-tracking simulation of a physical fire-spread model. *SIMULATION*, 86(10):629–646.

Finney, M. A. (1998). Farsite: Fire area simulator-model development and evaluation. Res. Pap. RMRS-RP-4, Revised 2004, Ogden, UT: U.S. Department of Agriculture, Forest Service, Rocky Mountain Research Station. 47 p.

Finney, M. A., Grenfell, I. C., McHugh, C. W., Seli, R. C., Trethewey, D., Stratton, R. D., and Brittain, S. (2011a). A method for ensemble wildland fire simulation. *Environmental Modeling & Assessment*, 16(2):153–167.

Finney, M. A., McHugh, C. W., Grenfell, I. C., Riley, K. L., and Short, K. C. (2011b). A simulation of probabilistic wildfire risk components for the continental united states. *Stochastic Environmental Research and Risk Assessment*, 25(7):973–1000.

Giuseppe, F. D., Vitolo, C., Krzeminski, B., Barnard, C., Maciel, P., and San-Miguel, J. (2020). Fire weather index: the skill provided by the european centre for medium-range weather forecasts ensemble prediction system. *Natural Hazards and Earth System Sciences*, 20(8):2365–2378.

Hardy, C. C. and Hardy, C. E. (2007). Fire danger rating in the united states of america: an evolution since 1916. *International Journal of Wildland*

Fire, 16(2):217–231.

Lac, C., Chaboureau, J.-P., Masson, V., Pinty, J.-P., Tulet, P., Escobar, J., Leriche, M., Barthe, C., Aouizerats, B., Augros, C., Aumond, P., Auguste, F., Bechtold, P., Berthet, S., Bielli, S., Bosseur, F., Caumont, O., Cohard, J.-M., Colin, J., Couvreux, F., Cuxart, J., Delautier, G., Dauhut, T., Ducrocq, V., Filippi, J.-B., Gazen, D., Geoffroy, O., Gheusi, F., Honnert, R., Lafore, J.-P., Brossier, C. L., Libois, Q., Lunet, T., Mari, C., Maric, T., Mascart, P., Mogé, M., Molinié, G., Nuissier, O., Pantillon, F., Peyrillé, P., Pergaud, J., Perraud, E., Pianezze, J., Redelsperger, J.-L., Ricard, D., Richard, E., Riette, S., Rodier, Q., Schoetter, R., Seyfried, L., Stein, J., Suhre, K., Taufour, M., Thouron, O., Turner, S., Verrelle, A., Vié, B., Visentin, F., Vionnet, V., and Wautelet, P. (2018). Overview of the meso-NH model version 5.4 and its applications. *Geoscientific Model Development*, 11(5):1929–1969.

Lawson, B. and Armitage, O. (2008). Weather guide for the canadian forest fire danger rating system. Natural Resources Canada, Canadian Forest Service, Northern Forestry Centre, Edmonton, Alberta. 84 p.

Parisien, M., Kafka, V., Hirsch, K., Todd, J., Lavoie, S., and Maczek, P. (2005). Mapping wildfire susceptibility with the BURN-P3 simulation model. Natural Resources Canada, Information Report NOR-X-405, Canadian Forest Service, Northern Forestry Centre, Edmonton, Alberta.

Parisien, M.-A., Dawe, D. A., Miller, C., Stockdale, C. A., and Armitage, O. B. (2019). Applications of simulation-based burn probability modelling: a review. *International Journal of Wildland Fire*, 28(12):913–926.

Rothermel, R. C. (1972). A mathematical model for predicting fire spread in wildland fuels. Res. Pap. INT-115. Ogden, UT: U.S. Department of Agriculture, Intermountain Forest and Range Experiment Station. 40 p.

Santambrogio, F. (2015). *Optimal Transport for Applied Mathematicians*, volume 87 of *Progress in Nonlinear Differential Equations and their Applications*. Birkhäuser / Springer, Cham.

Tymstra, C., Bryce, R., Wotton, B., Taylor, S., and Armitage, O. (2010). Development and structure of prometheus: the canadian wildland fire growth simulation model. Natural Resources Canada, Information Report NOR-X-417, Canadian Forest Service, Northern Forestry Centre, Edmonton, Alberta. 88 p.

Van Wagner, C. E. and Pickett, T. L. (1985). Equations and fortran program for the canadian forest fire weather index system. Forestry Technical Report No. 33. Ottawa, Environment Canada, Canadian Forestry Service, Petawawa National Forestry Institute.